REVIEW

Structure and function of enzymes in heme biosynthesis

Gunhild Layer,[1] Joachim Reichelt,[2] Dieter Jahn,[1]* and Dirk W. Heinz[2]*

[1]Institute of Microbiology, Technische Universität Braunschweig, Spielmannstrasse 7, Braunschweig D-38106, Germany
[2]Division of Structural Biology, Helmholtz Centre for Infection Research, Inhoffenstrasse 7, Braunschweig D-38124, Germany

Received 18 March 2010; Accepted 15 April 2010
DOI: 10.1002/pro.405
Published online 27 April 2010 proteinscience.org

Abstract: Tetrapyrroles like hemes, chlorophylls, and cobalamin are complex macrocycles which play essential roles in almost all living organisms. Heme serves as prosthetic group of many proteins involved in fundamental biological processes like respiration, photosynthesis, and the metabolism and transport of oxygen. Further, enzymes such as catalases, peroxidases, or cytochromes P450 rely on heme as essential cofactors. Heme is synthesized in most organisms via a highly conserved biosynthetic route. In humans, defects in heme biosynthesis lead to severe metabolic disorders called porphyrias. The elucidation of the 3D structures for all heme biosynthetic enzymes over the last decade provided new insights into their function and elucidated the structural basis of many known diseases. In terms of structure and function several rather unique proteins were revealed such as the V-shaped glutamyl-tRNA reductase, the dipyrromethane cofactor containing porphobilinogen deaminase, or the "Radical SAM enzyme" coproporphyrinogen III dehydrogenase. This review summarizes the current understanding of the structure–function relationship for all heme biosynthetic enzymes and their potential interactions in the cell.

Keywords: heme biosynthesis; enzymes; structure; metabolic pathway; porphyrin

Introduction

Tetrapyrroles like hemes and chlorophylls are molecules of central importance to essential metabolic processes, including electron transfer during respiration, photosynthesis, and enzyme catalysis. In this context, the iron-containing porphyrin heme fulfils widely diverse biological functions as prosthetic group for many enzymes, transporters, and receptors in most living organisms. Heme-containing cytochromes are integral components of various respiratory and photosynthetic electron transport chains. Heme serves as a prosthetic group in hemoglobin, myoglobin, catalases, peroxidases, cytochromes P450, and in sensor proteins for diatomic gases such as O_2 or NO.[1] In all eukaryotes and most prokaryotes, except the archaea and some eubacteria, heme is synthesized via a well established conserved biosynthetic pathway.[2] In humans, malfunction of this pathway leads to severe metabolic disorders, termed porphyrias.[3,4] The determination of the three-dimensional structures of all 11 heme biosynthetic enzymes within the last 15 years has led to a renaissance in the field of heme biosynthesis. Besides a significant gain in the overall understanding of this metabolic pathway, a number of novel

**Correspondence to:* Dieter Jahn, Institute of Microbiology, Technische Universität Braunschweig, Spielmannstrasse 7, Braunschweig D-38106, Germany. E-mail: d.jahn@tu-bs.de or Dirk W. Heinz, Division of Structural Biology, Helmholtz Centre for Infection Research, Inhoffenstrasse 7, Braunschweig D-38124, Germany. E-mail: dirk.heinz@helmholtz-hzi.de.

enzyme mechanisms have been unraveled. Examples include the unusual reduction of tRNA-bound glutamate by glutamyl-tRNA reductase, the dipyrromethane cofactor dependent oligomerization of porphobilinogen by porphobilinogen deaminase, and the employment of radical chemistry by coproporphyrinogen III dehydrogenase.

This review will focus on the structures and catalytic mechanisms of the following heme biosynthetic enzymes (Fig. 1): 5-Aminolevulinate synthase (ALAS), glutamyl-tRNA reductase (GluTR), glutamate-1-semialdehyde-2,1-aminomutase (GSAM), porphobilinogen synthase (PBGS), porphobilinogen deaminase (PBGD), uroporphyrinogen III synthase (UROS), uroporphyrinogen III decarboxylase (UROD), oxygen-dependent coproporphyrinogen III oxidase (CPO), coproporphyrinogen III dehydrogenase (CPDH, also known as oxygen-independent coproporphyrinogen III oxidase), oxygen-dependent protoporphyrinogen IX oxidase (PPO), and ferrochelatase (FC).

For each enzyme a brief historical overview on important discoveries is followed by the presentation of their three-dimensional structures and catalytic mechanisms. Amino acid exchanges caused by gene mutations implicated in human porphyrias are discussed in the light of the available structural information. Finally, the importance of interactions between a number of heme biosynthetic enzymes to achieve efficient transfer of metabolites is outlined.

Heme Biosynthesis

The biosynthesis of heme (Fig. 1) sets off with the formation of 5-aminolevulinic acid (ALA) as the common precursor for all naturally occurring tetrapyrroles. ALA represents the sole source of carbon and nitrogen atoms necessary for heme formation. Two ALA molecules are then condensed to the pyrrole porphobilinogen (PBG). Oligomerization of four PBG molecules to the linear tetrapyrrole intermediate pre-uroporphyrinogen (1-hydroxymethylbilane) followed by ring closure leads to the first cyclic tetrapyrrole intermediate uroporphyrinogen III (UROGEN). Next, the side chains of the macrocycle are modified resulting in the intermediates coproporphyrinogen III (COPROGEN) and protoporphyrinogen IX (PROTOGEN). Subsequently, the ring system is aromatized giving protoporphyrin IX (PROTO). Finally, iron is inserted to yield heme. Variations from this canonical pathway[5] occur in some bacteria and the archaea.[6–8]

Structures and Mechanisms of Heme Biosynthetic Enzymes

Heme biosynthesis can be divided into three parts: (i) formation of the precursor molecule ALA, (ii) formation of the first cyclic tetrapyrrole uroporphyrinogen III, and (iii) conversion of uroporphyrinogen III into heme.

Two ways lead to 5-aminolevulinic acid

5-Aminolevulinic acid (ALA) is synthesized in nature by two different, unrelated biosynthetic routes. The first one, discovered by Shemin, involves the condensation of glycine and succinyl-CoA by 5-aminolevulinic acid synthase (ALAS) and occurs in mammals, fungi, and α-proteobacteria. In plants, archaea and most bacteria the alternative course, termed "C_5-pathway," builds ALA from tRNA-bound glutamate in two steps. The initial substrate of the C_5-pathway, glutamyl-tRNA, is provided by glutamyl-tRNA synthetase and is shared between heme and protein biosyntheses. Glutamyl-tRNA reductase (GluTR) then converts glutamyl-tRNA in an NADPH-dependent reaction into the labile intermediate glutamate-1-semialdehyde which is then further transformed into ALA by glutamate-1-semialdehyde-2,1-aminomutase (GSAM).[9]

Shemin pathway

5-Aminolevulinic acid synthase (ALAS; EC 2.3.1.37) catalyzes the condensation of glycine and succinyl-CoA to yield ALA. During this reaction CO_2 and free coenzyme A are released. The first report about the incorporation of nitrogen atoms originating from glycine into heme was published in 1945, by Shemin and Rittenberg.[10] Ingestion of ^{15}N-labeled glycine over a 3-day-period led to ^{15}N-incorporation into Shemin's own heme. Further incorporation studies using radioactively labeled acetate performed by the Shemin and Neuberger groups led to the identification of succinyl-CoA as the second source of carbon atoms for heme formation in 1952.[11–13] After the identification of ALA as a potential precursor for heme biosynthesis,[14,15] ALA synthase (ALAS) activity in crude cell extracts was simultaneously described by the Shemin and Neuberger groups in 1958.[16–19] Since these early studies ALAS was purified from various eukaryotic and bacterial sources and biochemically characterized.[20] Whereas there is usually only one isoform of bacterial ALAS proteins, mammals carry two different ALAS isoforms, one of them fulfilling a housekeeping function (ALAS1) and the other sustaining high levels of heme biosynthesis in erythrocytes (ALAS2).[21] Mutations in the human erythroid-specific ALAS isoform lowering its catalytic activity are the cause of X-linked sideroblastic anemia which manifests in iron accumulation in erythroblast mitochondria.[22] On the other hand, an extremely high expression level of ALAS2 due to genetic alterations leads to the accumulation of protoporphyrin IX and causes X-linked dominant protoporphyria.[23] The only crystal structure of ALAS, from the phototrophic bacterium *Rhodobacter capsulatus*, was elucidated in 2005.[24]

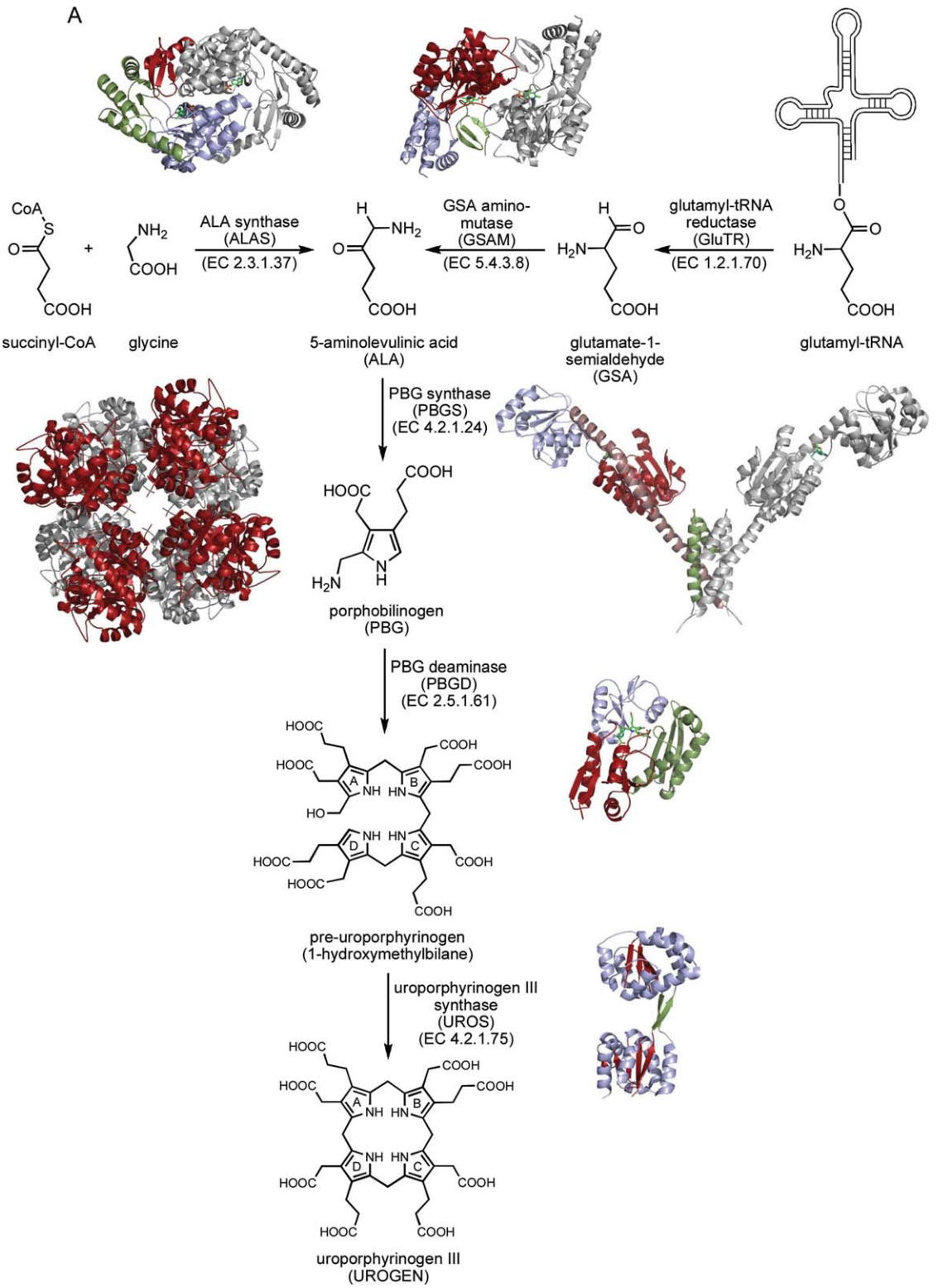

Figure 1. Heme biosynthesis. A: The first cyclic tetrapyrrole uroporphyrinogen III is formed from the precursor 5-aminolevulinic acid in three enzymatic steps via the intermediates porphobilinogen and pre-uroporphyrinogen. Depending on the organism, ALA is either synthesized by condensation of glycine with succinyl-CoA or from tRNA-bound glutamate via glutamate-1-semialdehyde. B: Uroporphyrinogen III is converted into heme in four consecutive enzymatic steps via the intermediates coproporphyrinogen III, protoporphyrinogen IX, and protoporphyrin IX. Structures of all heme biosynthesis enzymes have been determined with the exception of oxygen-independent PPO (n.d., structure not determined).

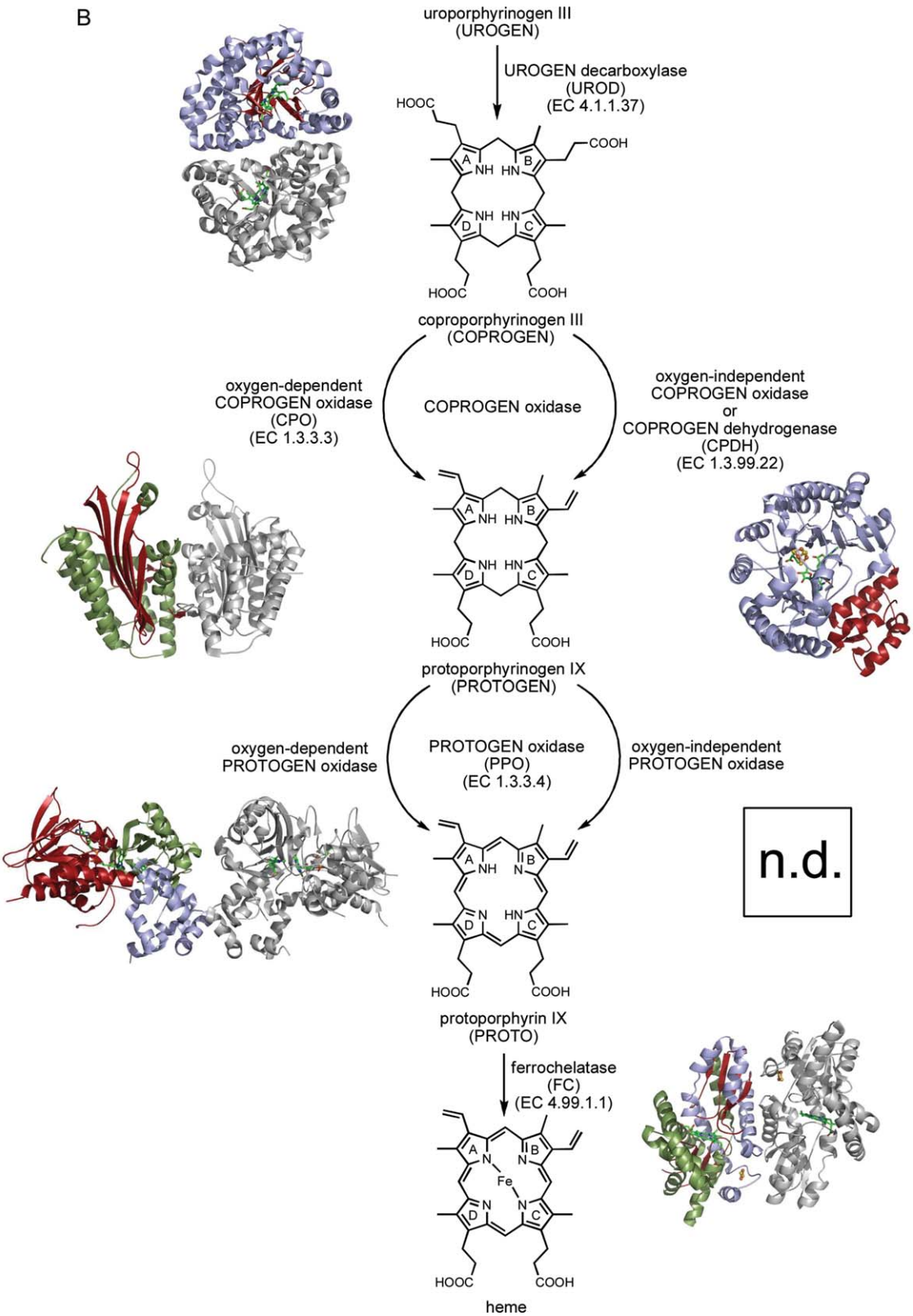

Figure 1. (Continued)

5-Aminolevulinic acid synthase

ALAS functions as a homodimer and requires the cofactor pyridoxal 5′-phosphate (PLP) for catalysis.[25,26] Within the family of PLP-dependent enzymes ALAS belongs to the subfamily of α-oxoamine synthases which catalyze the condensation of a carboxylic acid CoA thioester and small amino acids with concomitant decarboxylation of the latter.[27] The ALAS reaction mechanism is unusual for a PLP-dependent enzyme in that two α-carbon bonds

are cleaved during the reaction cycle. The current knowledge on the ALAS reaction mechanism was derived from various studies using specifically labeled substrates and extensive kinetic investigations using stopped-flow techniques, in combination with the available crystal structure of ALAS from *R. capsulatus*.[28–34] In the active form the PLP cofactor is covalently linked to an essential active site lysine residue via an internal aldimine. Catalysis begins with the binding of glycine to the active site and formation of an external aldimine between glycine and the PLP cofactor [Fig. 2 (A)]. Subsequently, the pro-*R* proton of glycine is removed by the active site lysine, succinyl-CoA is attached to the glycine α-carbon, and coenzyme A is released leading to an α-amino-β-keto adipate intermediate. Decarboxylation of this intermediate is achieved by a protonation step for which an active site histidine residue acts as general acid [Fig. 2(B)]. The formed enol intermediate is in equilibrium with a spectroscopically traceable quinonoid intermediate and with the ALA bound external aldimine upon protonation of the C-5 position. Finally, ALA is released and the internal aldimine restored.[35]

The crystal structures of *R. capsulatus* ALAS holoenzyme, in its free form as well as in complex with glycine and succinyl-CoA have provided detailed insights into the active site architecture [Fig. 2(A)].[24] Each subunit of the tightly interlocked ALAS homodimer consists of three domains (Fig. 1). The central catalytic domains of each monomer harbor the active site clefts located at the subunit interface. The active site pockets are deeply buried in the dimeric ALAS structure excluding water from the reaction to take place. Glycine and succinyl-CoA can enter the active site pocket through a narrow channel. PLP is precisely held in its binding site by various interactions with the surrounding amino acid residues. In the ALAS-glycine complex structure the substrate glycine replaces the active site lysine by forming the external aldimine with PLP. However, the lysine remains in a position suitable for proton abstraction from the PLP bound glycine. The structure of the ALAS-succinyl-CoA complex revealed that the 3′-phosphate ADP moiety of the stretched co-substrate binds to a hydrophobic pocket at the entrance of the active site channel on the surface of the enzyme and the succinate carboxylate group close to the PLP. An overlay of both substrate bound structures revealed a distance of ~2.8 Å between the C_α of PLP bound glycine and the CS1 of succinyl-CoA being poised for the required nucleophilic attack for C—C bond formation [Fig. 2(A)]. In all substrate bound structures a histidine, located directly above the PLP ring, could act as an acid promoting the decarboxylation of the α-amino-β-keto adipate intermediate.

Because of the high sequence conservation (49% identity) between *R. capsulatus* and human ALAS2 the structure of the bacterial enzyme can be used as a model for the mapping and analysis of point mutations causing X-linked sideroblastic anemia (XLSA). Some of the XLSA mutations are directly or indirectly affecting PLP or substrate binding. For example, Thr245 (Thr388 in human ALAS2) is involved in hydrogen bonding of the PLP phosphate group. When this residue is replaced by serine the patients suffer from a form of XLSA which can be treated by supplemental pyridoxine. In another XLSA mutation Arg517 (human ALAS2), which is crucial for glycine recognition and discrimination, is replaced by a cysteine.

C_5-Pathway

The second pathway leading to the formation of ALA was not discovered until the 1970s. By that time the Shemin pathway was well established, however all attempts to detect ALAS activity in extracts of green plants had failed. Furthermore, experiments with chlorophyll synthesizing tissues using labeled glycine did not result in the typical incorporation pattern as it was observed before for avian heme biosynthesis. In 1973, Beale and Castelfranco used various ^{14}C-labeled compounds to study the incorporation of the label into ALA by greening cucumber cotyledons. They observed that the metabolically related compounds glutamate, α-ketoglutarate and glutamine gave rise to ^{14}C-labeled ALA.[36] Two years later, it was found that the intact five-carbon skeleton of glutamate was incorporated into ALA.[37] It was shown only a few years later that glutamate was transformed into ALA via the reduced intermediate glutamate-1-semialdehyde (GSA) by detection of GSA aminotransferase activity in barley and the subsequent purification and characterization of the enzyme.[38,39] The next major discovery concerning the C_5-pathway in the mid-1980s was the finding that an RNA moiety was involved in the transformation of glutamate into ALA.[40] Finally, it was established that the initial metabolite of the C_5-pathway is Glu-tRNA^{Glu} which is reduced by glutamyl-tRNA reductase (GluTR, EC 1.2.1.70) to GSA which is then converted into ALA by glutamate-1-semialdehyde-2,1-aminomutase (GSAM, EC 5.4.3.8).[41,42] Since these early studies both enzymes were purified and characterized from various plant and bacterial sources.[43–52] The first crystal structure of GluTR was solved for the enzyme from *Methanopyrus kandleri* revealing an unusual V-shaped structure.[53] Crystal structures for GSAM were solved for the *Synechococcus* ($GSAM_{Syn}$) and the *Thermosynechococcus elongatus* enzyme ($GSAM_{Tel}$).[54,55]

Glutamyl-tRNA reductase

GluTR functions as a homodimeric, NADPH-dependent protein. The large tRNA substrate is recognized by its overall shape and NADPH binds to the

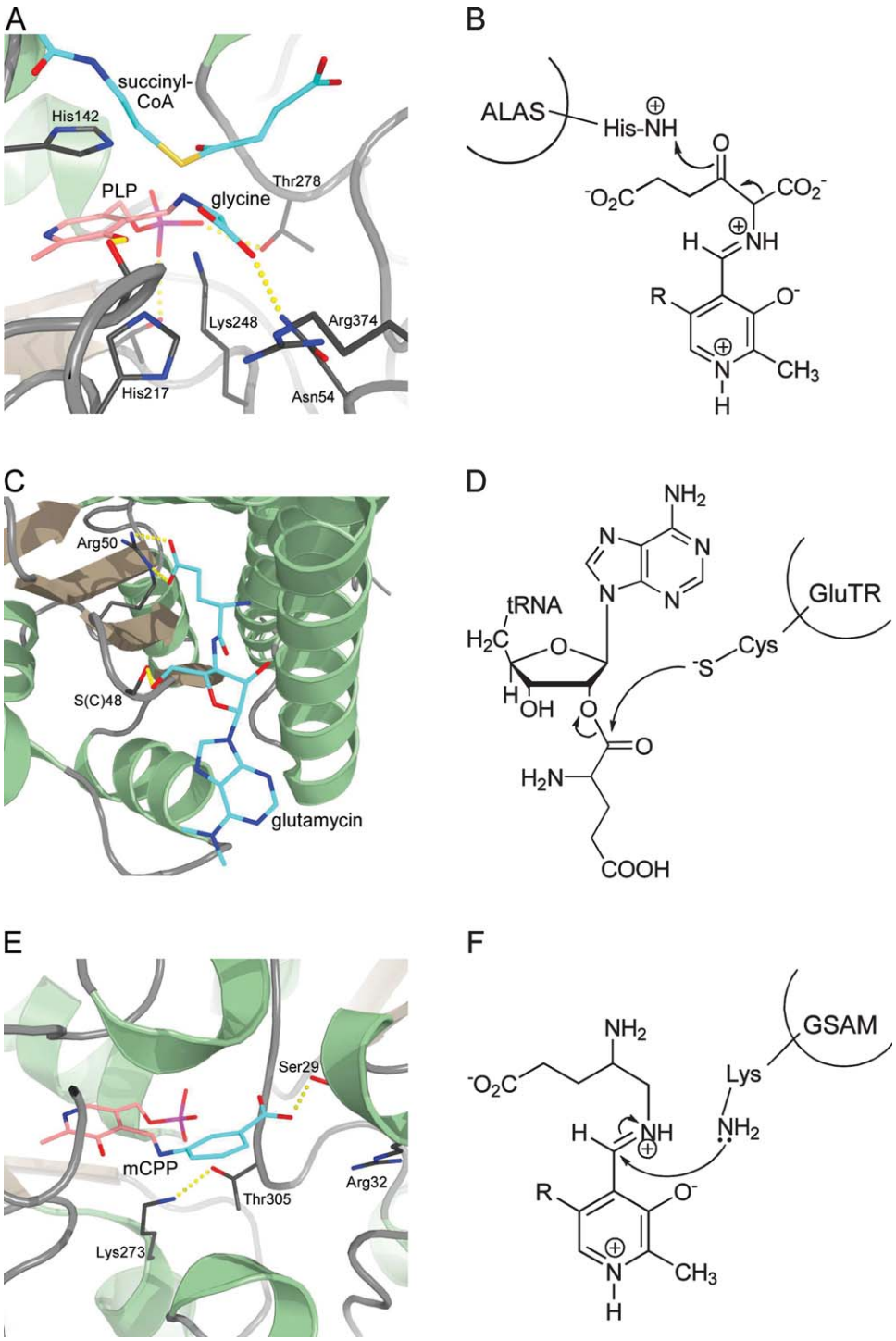

Figure 2. Active site architectures and catalytic steps of enzymes involved in ALA formation. A + B, ALAS; C + D, GluTR; E + F, GSAM. A: Active site of ALAS from *R. capsulatus* modeled from the glycine- and succinyl-CoA-bound structures showing the external aldimine between PLP and glycine in close proximity to the succinyl-CoA CS1 position. B: During the ALAS reaction cycle, the decarboxylation of the α-amino-β-keto adipate intermediate is promoted by His-mediated protonation. C: Active site of GluTR from *M. kandleri* with bound glutamycin and the catalytically essential Cys(Ser)48. D: During catalysis Cys48 nucleophilically attacks the activated α-carboxylate of the glutamyl-tRNA. E: Active site of GSAM from *Synechococcus* showing the inhibitor gabaculine covalently bound to the PLP cofactor resulting in the stable *m*-carboxyphenylpyridoxalamine phosphate (mCPP). F: The potential reaction intermediate 4,5-diaminovalerate covalently bound to PLP as an external aldimine.

enzyme with all its major determinants.[53,56,57] During catalysis a highly conserved cysteine residue located in the active site of the enzyme acts as a nucleophile attacking the activated α-carboxyl group of tRNA-bound glutamate [Fig. 2(C,D)]. This results in the release of the tRNA and formation of an

enzyme-bound thioester intermediate.[58] NADPH mediated hydride transfer to the thioester intermediate leads to the formation of glutamate-1-semialdehyde, while in the absence of NADPH the thioester bond is slowly hydrolyzed producing free glutamate.

The crystal structure of *M. kandleri* GluTR was solved in complex with the antibiotic inhibitor glutamycin and revealed an unusual V-shaped structure for the dimeric protein (Fig. 1).[53] Each monomer consists of three distinct domains which are arranged along a curved "spinal" α-helix linking domains II and III. The N-terminal domain I is located at the central part of the spinal helix and represents the catalytic domain. Domain II is located at the top of the extended helix and adopts a classical nucleotide-binding fold containing characteristic βαβ motifs and a conserved glycine rich loop. The dimerization domain III is located at the C-terminal end of the spinal helix and together with the corresponding domain of the second monomer forms an unusual six-helix bundle. Glutamycin was found to bind in a deep pocket of the catalytic domain. Several highly conserved amino acid residues specifically hold the inhibitor in its position. The glutamycin γ-carboxylate group is specifically recognized by a bidentate salt bridge with an arginine and two additional hydrogen bonds. Both the inhibitor α-amino group as well as the amide group of glutamycin are engaged in hydrogen bonds with the enzyme. Mutational analysis of these active site residues and kinetic characterization of the enzyme variants revealed their functional importance.[57] During catalysis Cys48 nucleophilically attacks the activated α-carboxylate of the glutamyl-tRNA. In the GluTR crystal structure Cys48 (replaced by a serine for technical reasons) is located in close proximity (3.9 Å) to the α-carbonyl carbon of glutamycin. The NADPH cofactor was modeled into the enzyme's nucleotide binding domain which was observed to be slightly compressed compared to other NADPH binding domains. From this model it was concluded that the observed GluTR conformation probably represented an open, pre-active state of the enzyme since NADPH was ~21 Å away from the glutamate binding pocket. It was suggested that upon glutamyl-tRNA binding a tipping of domain II towards domain I with a concomitant opening of the nucleotide binding pocket could be induced. The authentic substrate glutamyl-tRNA was also modeled into the GluTR structure revealing a striking surface complementarity between the enzyme and its unusual substrate. Functional identification of $tRNA^{Glu}$ identity elements for GluTR recognition showed the importance of the unique overall structure of the tRNA molecule.[56]

Glutamate-1-semialdehyde-2,1-aminomutase

GSAM belongs to the α-family of pyridoxal 5′-phosphate (PLP)-dependent enzymes and can be classified structurally and mechanistically as an aminotransferase. However, in contrast to other aminotransferases GSAM functions as aminomutase acting on a single substrate molecule. Two alternative mechanistic routes are conceivable for GSAM catalysis. The reaction starts either with enzyme bound pyridoxamine 5′-phosphate (PMP) or PLP and proceeds via the intermediates 4,5-diaminovalerate (DAVA) and PLP or 4,5-dioxovalerate (DOVA) and PMP, respectively.[59–61] All GSAM proteins studied so far are able to catalyze both reactions.[51,62] However, the first mechanism was found to be kinetically preferred and, therefore, DAVA was proposed to be the true reaction intermediate during GSAM catalysis.[63–65] GSAM acts as a functional homodimer as confirmed by X-ray crystallography (Fig. 1). Each monomer of the enzyme consists of three domains. The large central domains harbor the active sites which are located at the dimer interface. For the $GSAM_{Syn}$ structure an asymmetric homodimer was observed in which one subunit contained the cofactor in its PMP form whereas the second subunit contained PLP covalently linked to the active site lysine residue. Because of a lack of order for about 30 amino acid residues the PLP containing subunit was described to adopt an "open" conformation. In contrast, the same region was well ordered in the PMP binding subunit and covered the active site leading to a "closed" conformation. In contrast to these observations a symmetric homodimer was observed for the $GSAM_{Tel}$ structure in which both subunits were observed to adopt the "open" PLP bound form with the disordered region covering the active site. The PLP phosphate group is recognized via hydrogen bonds to surrounding amino acid residues and a water molecule. The PLP pyridinium ring is sandwiched between a valine and a tyrosine residue. In both GSAM structures a highly conserved arginine was observed ideally positioned to bind the carboxylate group of the substrate GSA. In a recent study the suicide inhibitor gabaculine was observed to bind covalently to the PLP cofactor resulting in a stable *m*-carboxyphenylpyridoxalamine phosphate form (mCPP).[66] The structure of the GSAM-inhibitor complex revealed that the cofactor rotates ~15° away from the active site lysine residue when compared to the PLP bound form of the enzyme. Further, the carboxylate group of gabaculine forms hydrogen bonds with the side chain of an active site serine and interacts with a nearby tyrosine and the conserved arginine via ordered water molecules [Fig. 2(E,F)].

Uroporphyrinogen III is formed from ALA in three consecutive enzymatic steps

Uroporphyrinogen III (UROGEN) represents the first cyclic intermediate of tetrapyrrole biosynthesis and at the same time the first major branch point for the diverging routes leading to formation of

different classes of tetrapyrroles.[5] This important intermediate is built from eight ALA molecules in three consecutive enzymatic steps. First, two ALA molecules are asymmetrically condensed by the enzyme porphobilinogen synthase (PBGS, EC 4.2.1.24, also known as ALA dehydratase) to yield the pyrrole derivative PBG. Next, four PBG molecules are linked together in a linear fashion by the enzyme porphobilinogen deaminase (PBGD, EC 2.5.1.61, also called hydroxymethylbilane synthase) yielding the linear tetrapyrrole pre-uroporphyrinogen (1-hydroxymethylbilane). Finally, UROGEN is formed from pre-uroporphyrinogen by the action of the enzyme uroporphyrinogen III synthase (UROS, EC 4.2.1.75). The heme precursor PBG was detected for the first time in the urine of a patient suffering from acute porphyria in 1931.[67] Shortly after its isolation and structure determination in 1952,[68,69] it was shown that PBG serves as an effective precursor for heme formation in avian red cells.[70] The hypothesis arose that an early step during heme biosynthesis could be the condensation of two ALA molecules to PBG[14,15] and finally the first purifications and characterizations of PBGS proteins from different sources in the mid-1950s provided proof for this proposal.[71,72] At about the same time it was found by Bogorad and Granick that the conversion of PBG into uroporphyrin III required the cooperative action of two enzymes and later these were identified as PBGD and UROS.[73,74] In the beginning of these early studies of heme biosynthesis the porphyrins uroporphyrin III, coproporphyrin III, and protoporphyrin IX were believed to be biosynthetic intermediates. However, in the mid-1950s it was established that the reduced forms of these porphyrins, the "porphyrinogens," are the true intermediates during heme biosynthesis.[75] Since these early studies PBGS, PBGD, and UROS proteins were purified from many different eukaryotic and prokaryotic sources and biochemically characterized.[76] Crystal structures of PBGS were solved much later for the enzymes from yeast, *E. coli* and *Pseudomonas aeruginosa* and *Chlorobium vibrioforme* with many of them containing inhibitors or reaction intermediates.[77–80] Structures for PBGD are available for the *E. coli* and human proteins.[81–83] The structure of human UROS was elucidated in 2001 followed by the *Thermus thermophilus* enzyme structure in complex with UROGEN.[84,85]

Porphobilinogen synthase

Porphobilinogen synthases usually function as homooctamers with the exception of the hexameric enzyme from *Rhodobacter capsulatus*.[86] Despite the high degree of amino acid sequence similarity between PBGSs from different organisms they are divided into subgroups according to their metal dependency. Human and yeast PBGS contain two zinc ions, one of them playing a role in catalysis, which are coordinated by highly conserved cysteine residues. *E. coli* PBGS also contains the active site zinc and an additional magnesium ion. *P. aeruginosa* PBGS does not require any zinc but contains magnesium ions at an allosteric site and monovalent cations in the active site. Finally, it was reported that some PBGS proteins are metal-independent.[86] In a series of biochemical and structural studies of PBGS using various substrate analogs and inhibitors the enzyme mechanism was elucidated.[87–96] In the first step, the ALA molecule which ultimately forms the propionate group of PBG (P-side ALA) binds to a highly conserved lysine residue within the so-called "P-site" of the enzyme via Schiff base formation. This is followed by the binding of the second ALA molecule (A-side ALA) giving rise to the acetate group of PBG to the "A-site," also covalently linked to another strictly conserved active site lysine residue [Fig. 3 (A,B)]. This second Schiff base at the A-site then undergoes transformation into an enamine as a prerequisite for the next catalytic step. In an aldole addition reaction the C3 atom of A-side ALA attacks the C4 of P-side ALA which results in formation of the C—C bond between the two ALA molecules. Next, the amino group of P-side ALA attacks the Schiff base at the C4 atom of A-side ALA which leads to C—N bond formation and release of the A-site lysine. Lysis of the remaining bond between the P-site lysine and the reaction intermediate is triggered by protonation of the former and possibly by conformational changes of the enzyme. Finally, proton abstraction leads to the aromatization and release of PBG.

The crystal structures of yeast, *P. aeruginosa*, and *E. coli* PBGS revealed that the octameric enzymes are composed of four dimers which are arranged around a central four-fold axis. Each monomer adopts the classical TIM-barrel fold with the active sites located at the C-terminal ends of the β-barrel. The active sites are covered by a flexible loop and thereby shielded from the surrounding medium. PBGS monomers contain an "N-terminal arm" which wraps around its dimeric partner. Recently, this "hugging" of the monomers was observed to be important for the formation of the functional octameric quarternary structure of PBGS, since human PBGS with a detached N-terminal arm was only able to form hexameric PBGS with low catalytic activity.[97] In the crystal structure of *P. aeruginosa* PBGS in complex with the inhibitor 5-fluorolevulinic acid (5F-LA) both 5F-LA molecules were observed to bind covalently to the lysine residues of the A- and P-sites, respectively [Fig. 3(A)].[93] In addition, the inhibitors are precisely positioned in the P- and A-site, respectively, through hydrogen bonds and hydrophobic interactions. Overall, the two active site lysine residues with the covalently bound inhibitor

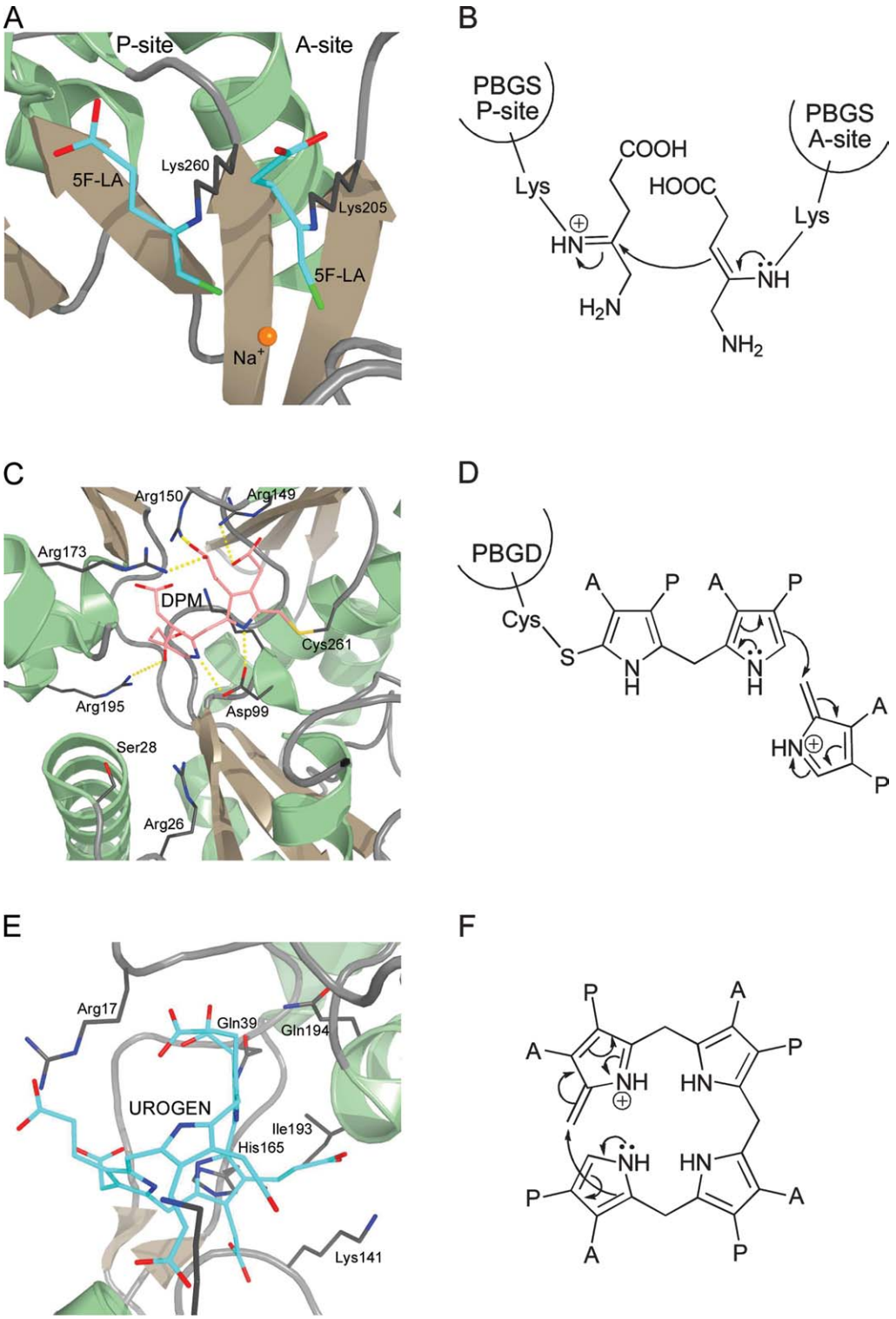

Figure 3. Active site architectures and catalytic steps of enzymes involved in uroporphyrinogen III formation. A + B, PBGS; C + D, PBGD; E + F, UROS. A: Active site of *P. aeruginosa* PBGS with bound inhibitor 5-fluorolevulinic acid (5F-LA). B: At the beginning of the PBGS reaction cycle both ALA molecules are covalently bound to the enzyme via Schiff bases to conserved lysine residues. C: Active site of human PBGD showing the unique dipyrromethane cofactor (DPM) covalently bound to an invariant cysteine residue. D: The oligomerization of PBG molecules proceeds via deaminated azafulvene intermediates. E: Active site of *T. thermophilus* UROS with bound uroporphyrinogen III (UROGEN) showing a puckered "two-up, two-down" conformation of the reaction product. F: Dehydration of pre-uroporphyrinogen results in the first azafulvene intermediate which further reacts to form a spirocyclic pyrrolenine intermediate as indicated by the arrows.

molecules are oriented roughly parallel to each other giving rise to two stacked T-shaped structures. A comparison of the 5F-LA conformations around their C3 atoms implies that enamine formation is facilitated for the A-site inhibitor molecule suggesting that the C—C bond formation through aldole condensation occurs prior to C—N bond formation.

In humans there are three distinct disorders due to decreased levels of PBGS activity of which only one is caused by mutations of the PBGS gene. PBGS porphyria is a very rare recessive autosomal disorder due to PBGS gene mutations and manifests with accumulation and urinary excretion of ALA and acute neurovisceral attacks. In cases of hepatorenal tyrosinemia a gene defect affecting the last step of tyrosine catabolism leads to the accumulation of succinylacetone which is a potent inhibitor of PBGS. Finally, lead poisoning also leads to inhibition of PBGS due to the replacement of the catalytically essential zinc ions of human PBGS by the toxic metal.[3] Bacterial PBGS provides a target for antibiotic therapy as revealed by the recent structure of *P. aeruginosa* PBGS in complex with the antibiotic alaremycin.[98]

Porphobilinogen deaminase

It was found around 1980 in a series of studies using labeled PBG, that first a linear tetrapyrrole is formed followed by ring closure with rearrangement of ring D.[99,100] At that time it was also observed that the oligomerization of PBG starts with ring A followed by rings B, C, and D.[101,102] Finally, 1-hydroxymethylbilane (pre-uroporphyrinogen) was identified by the groups of Scott and Battersby to be the reaction product of the enzyme now known as porphobilinogen deaminase.[103–105] Another major progress for the understanding of the PBGD protein was the discovery by Jordan and Warren and Battersby's group that the enzyme contains a covalently attached unique dipyrromethane cofactor consisting of two linked PBG molecules [Fig. 3(C,D)].[106–108] This cofactor serves as a primer for the oligomerization of another four PBG molecules resulting in the formation of a protein bound linear hexapyrrole. From this precursor the linear tetrapyrrole pre-uroporphyrinogen is then cleaved off leaving the free enzyme with its dipyrromethane cofactor behind.[109] During catalysis, a highly conserved aspartate residue plays an important role probably by assisting in the deamination of incoming PBG molecules.[81,110] The formed reactive azafulvene intermediate can then react with the protein bound oligopyrrole [Fig. 3(D)]. Although it is not yet clear how exactly the enzyme deals with the growing oligopyrrole chain during catalysis a number of conserved arginine residues seems to be involved in the correct positioning of the dipyrromethane cofactor and the incoming PBG molecules. Further, it was observed that the protein undergoes conformational changes during catalysis which might help the enzyme in "pulling" the oligopyrrole through the active site or alternatively being caused by the reorganization of the oligopyrrole as it is formed.[111] Mutations in human PBGD can cause acute intermittent porphyria (AIP), an inherited autosomal dominant disorder which manifests with attacks of abdominal pain and neurological symptoms accompanied by elevated levels of ALA and PBG in the patients' urine.

The crystal structures of *E. coli* and human PBGD revealed a monomeric protein consisting of three equally sized α/β domains with a high degree of flexibility in terms of domain movements.[81–83] The N-terminal domain I and the central domain II adopt a fold similar to transferrins and some bacterial periplasmic binding proteins. Domain III consists of a three-stranded, anti-parallel β-sheet decorated on one side by three α-helices and interacts both with domains I and II. The large active site cleft is located at the interface between domains I and II and is predominantly positively charged. The dipyrromethane cofactor is covalently bound to the enzyme via a thioether linkage to a conserved cysteine which resides on a loop of domain III. The cofactor is positioned in the active site by various ionic interactions between the carboxylate groups of its acetate and propionate side chains to conserved arginine and lysine residues. The catalytically essential aspartate forms hydrogen-bonds to both pyrrole NH-groups of the cofactor [Fig. 3(C)]. The proposed active site of PBGD was occupied by an acetate ion in the *E. coli* PBGD structure and a sulfate ion in the human PBGD structure. The sulfate ion was located in hydrogen-bonding distance to an arginine and a serine which were proposed to be involved in substrate binding. Indeed, a mutation involving this arginine results in AIP in humans. Further mutations leading to AIP involve arginine residues being involved in cofactor assembly and positioning or substrate binding. In total, there are more than 100 known mutations causing AIP in humans either due to less stable or truncated forms of the protein or defects in cofactor and substrate binding.

Uroporphyrinogen III synthase

UROS catalyzes the cyclization of the linear tetrapyrrole pre-uroporphyrinogen to uroporphyrinogen III under inversion of ring D. Although the first purification of an UROS protein dates back to 1957 it took another 20 years until the actual substrate, pre-uroporphyrinogen, of this enzyme was identified. However, in 1961 a mechanism for the formation of UROGEN was proposed by Mathewson and Corwin which has stood the test of time.[112] Studies using ^{13}C-labeled PBG and NMR spectroscopy, investigations employing synthetic spirocyclic inhibitors as well as the trapping of an azafulvene reaction

intermediate contributed to the current understanding of the UROS catalytic mechanism.[113–115] In the first steps of catalysis the hydroxyl group on ring A of pre-uroporphyrinogen is lost as a water molecule resulting in formation of the first azafulvene intermediate [Fig. 3(F)]. Next, the spirocyclic pyrrolenine intermediate is formed by reaction of the azafulvene with the substituted α-position of ring D. Bond breakage between rings C and D then leads to formation of the second azafulvene intermediate on ring C. In the final steps of catalysis the enzyme has to orientate the ring D pyrrole in such a way that the C ring azafulvene can react with its free α-position. Finally, deprotonation and bond rearrangements lead to the formation of UROGEN.

In addition to the crystal structure of human UROS the structure of *T. thermophilus* UROS in complex with its reaction product UROGEN was obtained only recently.[84,85] Despite a rather low level of amino acid sequence identity of only 14% between human and *T. thermophilus* UROS the overall fold of the enzymes from the two different organisms was found conserved. UROS is a monomeric protein which consists of two α/β domains connected by a flexible, two-stranded linker (Fig. 1). Domain I belongs to the flavodoxin-like fold family and domain II adopts a DNA glycosylase-like fold. In the human UROS structure the linker connecting the two domains adopts an antiparallel β-ladder conformation. In contrast, *T. thermophilus* UROS crystallized in several different conformations in which the linker is much less ordered than in the human UROS structure. The observed remarkable array of different domain-domain orientations suggests the linker being highly mobile in solution in the absence of the substrate.[85] In the crystal structure of the *T. thermophilus* UROS-product complex it was observed that uroporphyrinogen III binds at the interface between domains I and II and that the two domains approach each other more closely than in the different apo-UROS structures. The porphyrinogen adopts a puckered "two-up, two-down" conformation in which the pyrrole NH-groups of rings A and C point in one direction and those of rings B and D in the opposite direction [Fig. 3(E)]. Only few hydrophobic interactions between the enzyme and the pyrrole rings D and B were observed. The pyrrole NH-groups do not directly interact with the enzyme but rather form hydrogen bonds with ordered water molecules, while the carboxylate groups of the acetate and propionate substituents form hydrogen bonds with main chain NH-groups. Most of these hydrogen bonds involve the acetate and propionate side chains of rings A and B which are thus precisely positioned in a constrained conformation within the "closed" form of the active site. This is consistent with the observation that substrate binding is abolished for porphyrinogens in which the ring A or B substituents are altered.[116,117] For the ring C substituents there are hydrogen bonds between the propionate carboxylate group and main chain NH-groups whereas the acetate side chain does not directly interact with the protein. Likewise, the carboxylate groups of the ring D side chains do not interact with the enzyme facilitating the ring flip during the reaction.

Mutations in human UROS cause congenital erythropoietic porphyria (CEP) which is characterized by the accumulation of uroporphyrin I in the patients' urines and severe photosensitivity. Most of the known CEP mutations reduce the enzyme's activity by reducing its stability by disrupting the overall structural integrity. For a long time identification of plant UROS failed due to the low degree of amino acid sequence conservation. Recently, the *Arabidopsis thaliana* enzyme was identified and characterized as a typical UROS.[118]

Conversion of uroporphyrinogen III into heme requires four enzymatic steps

During the conversion of uroporphyrinogen III into heme the side chains of the macrocycle are modified, the tetrapyrrole ring system is oxidized, and finally iron is inserted. Uroporphyrinogen III decarboxylase (UROD, EC 4.1.1.37) catalyzes the stepwise decarboxylation of the four acetic acid chains of UROGEN to yield the corresponding methyl groups of coproporphyrinogen III. COPROGEN is then oxidatively decarboxylated yielding protoporphyrinogen IX by the action of either oxygen-dependent coproporphyrinogen III oxidase (CPO, EC 1.3.3.3) or oxygen-independent CPO which should rather be named coproporphyrinogen III dehydrogenase (CPDH, EC 1.3.99.22). In the penultimate step of heme biosynthesis, PROTOGEN is oxidized to PROTO by oxygen-dependent or -independent protoporphyrinogen IX oxidase (PPO, EC 1.3.3.4) before, finally, iron is inserted into the macrocycle by ferrochelatase (FC, EC 4.99.1.1) yielding heme.[119] The oxidized forms of the pathway intermediates, uroporphyrin III, coproporphyrin III, and protoporphyrin IX, are found in unusual high amounts in the urines of patients suffering from different porphyrias. Early descriptions of such porphyrin accumulations date back to the middle of the 19th century and were followed by the isolation and characterization of these porphyrins providing first hints for heme biosynthetic intermediates. The enzymes UROD, CPO and CPDH, PPO, and FC were subsequently purified from various eukaryotic and prokaryotic sources and the corresponding genes were cloned and sequenced.[120–122] Crystal structures are available for human UROD in its apo and COPROGEN bound forms, as well as for *Nicotiana tabacum* and *Bacillus subtilis* UROD.[123–126] CPO was crystallized and the structures solved for the yeast and human enzymes.[127,128]

The structure of *E. coli* CPDH was reported in 2003.[129] The first structure of PPO was obtained for the tobacco protein followed by structures of *Myxococcus xanthus* and *B. subtilis* PPOs.[130–132] Ferrochelatase was structurally characterized for the water soluble *B. subtilis* protein, the membrane attached human enzyme and the yeast FC followed by various structures of FC variants and of FC in complex with substrate and inhibitors.[133–136]

Uroporphyrinogen III decarboxylase

UROD activity was first described in 1958 by Mauzerall and Granick.[137] In 1976, it was proposed that the four decarboxylation reactions occur sequentially in a clockwise manner starting with the acetate side chain on ring D followed by those on rings A, B, and C.[138] This was substantiated by studies in which different partially decarboxylated intermediates accumulating in the urines of patients suffering from porphyria cutanea tarda (PCT) as a result of diminished UROD activity were analyzed.[139] PCT is the most common form of porphyria in humans which occurs with an estimated frequency of 1 in 20,000 Caucasians. UROD proteins were purified from many species including bacteria, yeast, and human.[140] It was found that UROD accepts a wide variety of different substrates including uroporphyrinogens I and III as well as all 14 possible intermediates between UROGEN and COPROGEN.[141] Accordingly, at high substrate concentrations the four decarboxylation reactions take place randomly.[142] UROD represents an unusual decarboxylase in that it is not dependent on any prosthetic group or cofactor. In a recent study the decarboxylation reaction catalyzed by UROD was described as a "benchmark for the catalytic proficiency of enzymes" due to the enormous rate enhancement of substrate decarboxylation by this enzyme.[143] The solved crystal structures for UROD proteins revealed a dimeric enzyme in which the two single-domain subunits are orientated head-to-head with the active site clefts facing each other at the dimer interface (Fig. 1). This arrangement of the two monomers results in one large active site well shielded from the surrounding solvent. On the basis of these structural observations two possible scenarios for the sequential decarboxylation of the four acetate side chains of UROGEN have been put forward. In one of these proposals, the acetate side chain of ring D is first decarboxylated in the active site of one monomer, the resulting intermediate then passed to the active site of the other monomer where the three remaining decarboxylation reactions on rings A, B, and C take place, making the 180° flipping of the substrate superfluous.[125] However, recently it was shown using a dimeric, single-chain UROD construct and variants thereof, that substrate shuttling between the active sites of UROD is not required to generate COPROGEN,[144] suggesting a reorientation of the substrate by only 90° for each decarboxylation which is in agreement with the crystal structure of human UROD in complex with its reaction product COPROGEN bound in a dome-shaped conformation.[124] This conformation placed the four central NH-groups of the tetrapyrrole in hydrogen bonding distance to a highly conserved aspartate residue being proposed to be involved in substrate binding and catalysis [Fig. 4 (A)]. According to this mechanism, the substrate pyrrole ring is first protonated at the α-position adjacent to the C atom bearing the acetate side chain. This protonation is promoted by the aspartate residue by stabilizing the positively charged reaction intermediate and possibly by acting as the conjugate acid directly donating the required proton [Fig. 4(B)].[143] Decarboxylation of the acetate side chain yields another reaction intermediate which has to be protonated at the methylene carbon and deprotonated at the α-C atom to yield the reaction product. It was suggested that a highly conserved arginine residue within the active site could be involved in the final protonation step.[143] After reorientation of the substrate by 90° the next decarboxylation takes place in the same active site following the same mechanistic strategy.

The UROD-product complex represented the first crystal structure which contained a highly oxygen-sensitive porphyrinogen.[124] The UROD reaction product COPROGEN was observed to bind in the active site cleft in a dome-shaped conformation with one face of the tetrapyrrole nestled up against a ring of conserved hydrophobic amino acid residues. In the observed conformation, the pyrrole rings A, B, and D are tilted 35–60° from the plane whereas ring C lies approximately in the plane of the four central NH-groups. As a result thereof the ring A, B, and D amines are positioned in an optimal distance for hydrogen-bonding with one of the γ-carboxylate oxygen atoms of the catalytically essential aspartate which is precisely positioned above the tetrapyrrole. The propionate side chains of COPROGEN are coordinated by conserved arginine residues within the active site. These arginines do, however, rather provide a favorable positively charged environment to accommodate the negatively charged substrate instead of precisely orienting the porphyrinogen, thus explaining the enzyme's ability to accept a large array of different substrates.

Coproporphyrinogen III oxidase

The conversion of coproporphyrinogen III into protoporphyrinogen IX requires the oxidative decarboxylation of the propionate side chains on rings A and B of the tetrapyrrole to yield the corresponding vinyl groups. This reaction is catalyzed by enzymes which are generally named coproporphyrinogen III oxidases. However, depending on the requirement for

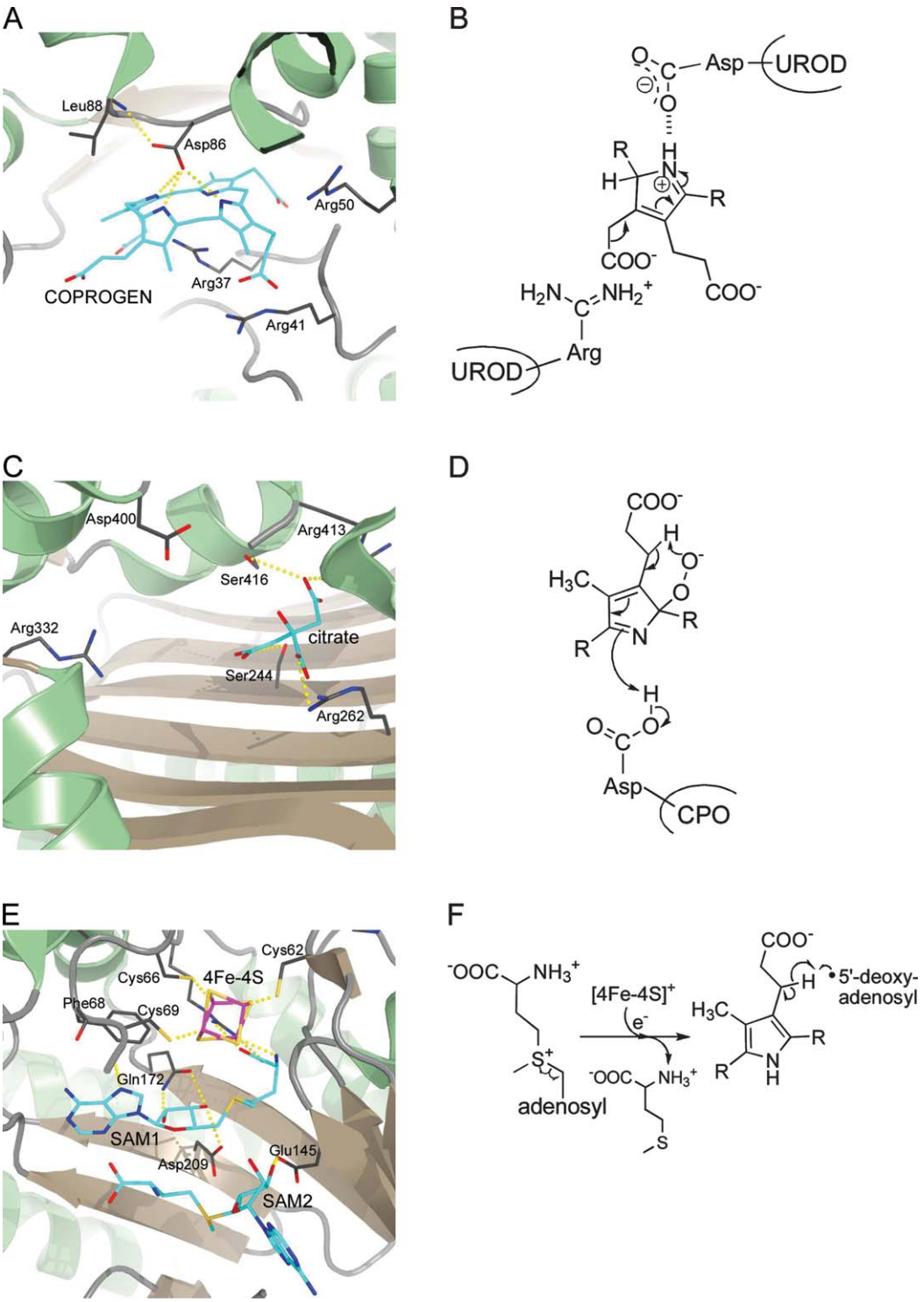

Figure 4. Active site architectures and catalytic steps of enzymes involved in protoporphyrinogen IX formation. A + B, UROD; C + D, CPO; E + F, CPDH. A: Active site of human UROD with bound coproporphyrinogen III (COPROGEN) in a dome-shaped conformation showing the catalytically essential aspartate in hydrogen bonding distance to the pyrrole NH-groups. B: The aspartate residue stabilizes the protonated, positively charged reaction intermediate. C: Active site of human CPO with bound citrate showing several arginine residues possibly involved in substrate binding and the catalytically essential aspartate. D: During catalysis, a pyrrole peroxide anion is formed which further reacts via proton abstraction through the peroxide to form an intermediate containing an exocyclic double bond. E: Active site of *E. coli* CPDH showing the catalytically essential [4Fe-4S] cluster and the two bound SAM molecules. F: During the initial reaction steps the reduced iron-sulfur cluster transfers an electron to SAM, which is thereby cleaved into methionine and a 5′-deoxyadenosyl radical. This radical then abstracts a hydrogen atom from the substrate propionate side chain resulting in the formation of 5′-deoxyadenosine and a substrate radical. R = tetrapyrrole.

molecular oxygen as terminal electron acceptor there are two distinct types of CPO which are structurally and mechanistically completely unrelated proteins. In this review, we will refer to the oxygen-dependent enzyme as CPO whereas we will name the oxygen-independent protein coproporphyrinogen III dehydrogenase (CPDH).

CPO is mainly found in eukaryotes with only few described bacterial representatives.[145] Decreased activity of CPO in humans manifests in the autosomal dominant hereditary coproporphyria.[146] The first partial purification of CPO was reported in 1961 by Sano and Granick for the bovine liver enzyme.[147] This was followed 4 years later by the partial isolation of the enzyme from rat liver by Battle *et al*. and in the mid-1970s by the purification of yeast CPO by Poulson and Polglase.[148,149] Since these early studies a number of native and recombinant CPO proteins were purified to homogeneity and biochemically characterized.[150–155] CPO functions as a dimeric protein which requires molecular oxygen as the terminal electron acceptor during catalysis. It was shown that CPO catalyzes the decarboxylation of the ring A propionate side chain prior to that on ring B under formation of the reaction intermediate harderoporphyrinogen.[156,157] Early stereochemical and mechanistic studies using deuterium and tritium-labeled substrates showed that only the pro-*S*-hydrogen atom at the β-carbon of the substrate propionate side chain is removed during the reaction and that the overall conversion of propionate side chains into vinyl side chains occurs stereochemically by antiperiplanar elimination.[158–160] Recently, a putative reaction mechanism was proposed for the oxygen-dependent decarboxylation of COPROGEN and evaluated by quantum chemical treatments.[161,162] In this proposal the first step is a base catalyzed deprotonation of the pyrrole NH-group yielding an azacyclopentadienyl anion. This anion then reacts with molecular oxygen at the α-position to form a pyrrole peroxide anion [Fig. 4(D)]. Next, a proton at the β-position of the substrate propionate side chain is abstracted by the peroxide via a six-membered ring transition state resulting in an exocyclic double bond. Finally, elimination of CO_2 and H_2O_2 and bond rearrangements lead to formation of the vinyl group. Indeed, it was shown in a recent study that H_2O_2 is generated during CPO catalysis.[155] Unfortunately, the two solved crystal structures for CPO did not contain substrate or product precluding a precise assignment of amino acid residues directly involved in catalysis.[127,128] However, in a recent biochemical study employing mutant human CPOs it was suggested that a highly conserved aspartate residue might serve as the base for NH proton abstraction, and two conserved arginine residues were proposed to coordinate the substrate carboxylate groups.[163]

Both yeast and human CPO structures confirmed the dimeric state of the protein.[127,128] Each monomer consists of a single domain adopting an unprecedented fold containing a large seven-stranded antiparallel β-sheet covered on both sides by α-helices. In the homodimer the two β-sheets of the monomers face each other and the subunits are rotated by ~40° relative to one another (Fig. 1). A putative active site cleft was localized matching the size of the substrate [Fig. 4(C)]. Interestingly, yeast CPO crystallized in two different crystal forms. The structures revealed that in one of these forms the active site cleft was in an open, accessible conformation whereas in the second form the active site was covered by one of the α-helices leading to a cavity well shielded from the solvent. Two invariant arginine residues were found to point their side chains into the active site cavity suggesting interactions with the substrate's propionate side chains. An invariant aspartate residue which exposes its side chain to the cavity near the centre of one face was proposed to coordinate the pyrrole NH-groups similar to the UROD-product complex structure.

Mutations in human CPO cause the autosomal dominant disease hereditary coproporphyria (HCP). Most of the >20 known clinically identified HCP mutations cause a decreased overall stability of the protein. Some mutations located in the active site cavity, like that of an invariant arginine and serine, are thought to have deleterious effects due to altering the size, shape and polarity of the active site.[128]

Coproporphyrinogen III dehydrogenase

In most bacteria, the conversion of COPROGEN into PROTOGEN is catalyzed by coproporphyrinogen III dehydrogenase. CPDH uses a terminal electron acceptor other than oxygen for the oxidative decarboxylation reaction. The first reports describing CPDH activity in cell free extracts prepared from *Rhodobacter sphaeroides* were published around 1970 by Tait.[164,165] Ten years later, it was found that the oxygen-independent conversion of COPROGEN into PROTOGEN proceeds with the same stereochemistry as the oxygen-dependent reaction and that only the pro-*S*-hydrogen atom at the β-carbon of the substrate propionate side chain is lost.[159] However, all these studies did not result in the isolation or characterization of the protein(s) responsible for the reaction. In the 1990s, genetic approaches finally led to the identification of CPDH encoding genes from various bacteria and these were cloned and sequenced.[166–170] Subsequently, recombinant CPDH from *E. coli* was purified to homogeneity and biochemically and structurally characterized. CPDH is a monomeric protein which belongs to the so-called "Radical SAM" protein family. As such it contains an oxygen-labile [4Fe-4S] cluster in which three iron atoms are coordinated by three highly

conserved cysteine residues of the characteristic CX_3CX_2C motif.[171] The fourth iron atom of the FeS cluster is ligated by an *S*-adenosyl-L-methionine (SAM) molecule which serves as a cofactor by initiating radical based catalysis.[129] The CPDH reaction cycle starts with the reduction of the FeS centre by an as yet unidentified electron donor system such as flavodoxin/flavodoxin reductase. The reduced iron-sulfur cluster then transfers the electron to bound SAM which is thereby homolytically cleaved into methionine and a 5′-deoxyadenosyl radical [Fig. 4(F)]. This highly reactive radical then abstracts a hydrogen atom from the substrate propionate side chain resulting in the formation of 5′-deoxyadenosine and an allylic substrate radical.[172] Finally, elimination of CO_2 and transfer of the remaining single electron to an as yet unidentified terminal electron acceptor completes the CPDH reaction cycle. It was found that during formation of one PROTOGEN molecule two SAM molecules are cleaved.[173] Interestingly, two SAM molecules were bound in the crystal structure of the *E. coli* enzyme providing the possibility that both decarboxylation reactions can take place without the need for release of a tricarboxylic acid intermediate from the active site.

The overall structure of CPDH revealed a monomeric, two domain protein (Fig. 1).[129] The larger N-terminal domain consists of a curved, twelve-stranded, largely parallel β-sheet which is decorated at its outer surface by α-helices. The central core of this domain is formed by the six N-terminal β-strands which are part of a curved $(\beta/\alpha)_6$ repeat. This $(\beta/\alpha)_6$ repeat structurally resembles known TIM barrel domains, however, in the CPDH structure the β-strands are less strongly inclined relative to the barrel axis and the curvature is not as tight as in known TIM barrel structures leading to a three-quarter barrel with a lateral opening. The C-terminal domain consists of a bundle of four α-helices and a small three-stranded antiparallel β-sheet. The first 35 amino acid residues of the protein belong to neither of the two domains and are only partially ordered. Since several conserved amino acid residues are located within this N-terminal stretch it was proposed that it might adopt a fully ordered conformation upon substrate binding. The [4Fe-4S] cluster is located at the centre of the three-quarter barrel near the C-terminal ends of the β-strands. Two SAM molecules are bound in close proximity to the iron-sulfur cluster with one of them acting as the fourth ligand to the FeS-cluster [Fig. 4(E)]. Based on a modeled CPDH-substrate complex several conserved arginine residues were proposed to interact with the substrate's propionate substituents. Any definite conclusions concerning the sequence of the two successive decarboxylation events were not possible. However, very recently it was reported that CPDH, like CPO, catalyzes the decarboxylation of the ring A propionate side chain prior to that on ring B via the reaction intermediate harderoporphyrinogen.[174]

Protoporphyrinogen IX oxidase

In the penultimate step of heme biosynthesis protoporphyrinogen IX is oxidized to protoporphyrin IX. Although this oxidation also occurs on its own, it was found in early studies in the early 1960s that *in vivo* this reaction is catalyzed by protoporphyrinogen IX oxidase.[147,175,176] As is the case for CPO there are also two distinct, unrelated PPO proteins catalyzing the six electron oxidation of PROTOGEN. Oxygen-dependent PPO uses molecular oxygen as the terminal electron acceptor whereas oxygen-independent PPO shuttles the electrons to anaerobic respiratory chains with alternative terminal electron acceptors such as nitrate or fumarate.[177,178] In the late 1980s, native oxygen-dependent PPO proteins were purified to homogeneity from bovine liver, mouse liver, and yeast later followed by recombinant PPOs from eukaryotic sources.[179–183] Bacterial oxygen-dependent PPOs were purified and characterized from *Bacillus subtilis*, *Myxococcus Xanthus*, and the thermophilic bacterium *Aquifex aeolicus*.[184–186] Mutations in the *ppo* gene in humans lead to the dominantly inherited disorder variegate porphyria (VP). Oxygen-dependent PPOs are usually homodimeric, membrane-associated proteins with the exception of monomeric PPO from *B. subtilis* and *A. aeolicus*.[132,186] In addition, *B. subtilis* PPO was found to be soluble in the cytoplasm.[187] In all cases oxygen-dependent PPOs contain an FAD cofactor which transfers the electrons from the substrate to the electron acceptor oxygen. During the whole reaction three O_2 molecules are thus reduced to three H_2O_2 molecules. On the basis of the results of biochemical studies using tritium-labeled substrates a reaction mechanism was proposed in which three *meso*-carbon hydride ions are removed successively from the same face of the macrocyclic plane, each accompanied by the loss of an NH proton. The final tautomerization leading to PROTO then occurs through the stereospecific loss of the remaining *meso*-carbon hydrogen as a proton from the opposite face of the tetrapyrrole plane.[121] In a recent mechanistic proposal based on the modeled enzyme-substrate complex of tobacco PPO all three hydride abstractions occur from the C20-*meso*-carbon followed by hydrogen rearrangements via enamine-imine tautomerizations which take place over the whole ring system.[130]

The crystal structures for mitochondrial tobacco PPO and the PPOs from *M. xanthus* and *B. subtilis* revealed that the overall fold of the protein is conserved despite a low degree of amino acid sequence conservation (~27% identity). Each monomer of dimeric tobacco and *M. xanthus* PPO and monomeric *B. subtilis* PPO consists of three domains, an FAD-binding, a substrate-binding and a third domain

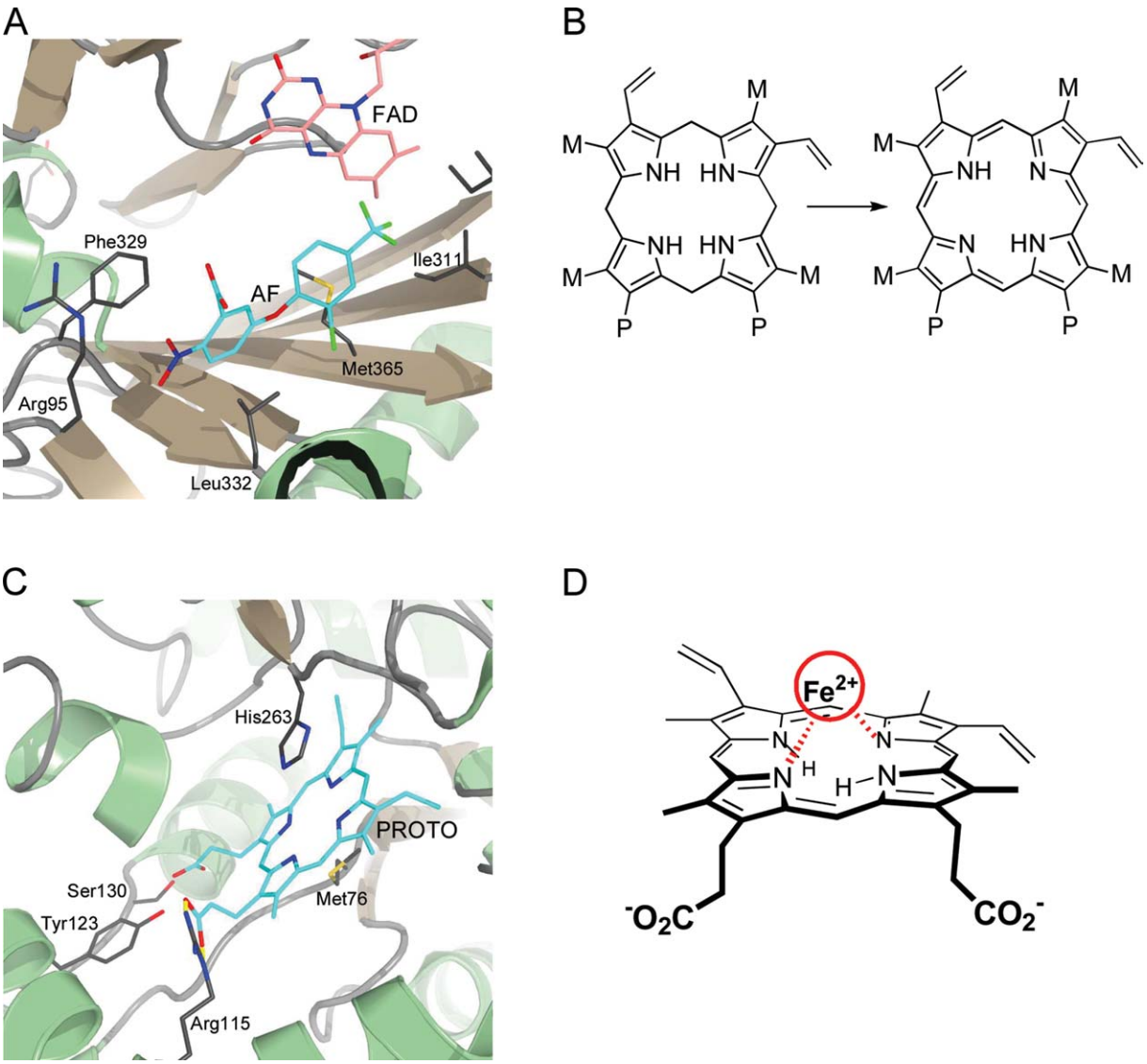

Figure 5. Active site architectures and catalytic steps of enzymes involved in the transformation of protoporphyrinogen IX into heme. A + B, PPO; C + D, FC. A: Active site of *M. xanthus* PPO with bound inhibitor acifluorfen (AF). B: PPO catalyzes the oxidation of protoporphyrinogen IX to protoporphyrin IX. C: Active site of human FC with bound protoporphyrin IX (PROTO). D: The insertion of ferrous iron into PROTO proceeds via a "sitting-atop" complex between the porphyrin and the metal ion.

involved in dimerization in the case of tobacco and *M. xanthus* PPO (Fig. 1). The FAD-binding and substrate-binding domains show a *p*-hydroxybenzoate-hydroxylase fold-like topology. The dimerization domain is exclusively α-helical and responsible for membrane-binding in the case of the tobacco and *M. xanthus* enzymes. Conformational differences were observed for this domain in the *B. subtilis* protein explaining the different oligomerization states of the different PPOs. On the basis of the localization of inhibitor molecules in the PPO structures the active site of PPO was identified [Fig. 5 (A)]. Whereas in tobacco and *M. xanthus* PPO the substrate binding site is a shallow cavity, it is much wider in the *B. subtilis* PPO structure explaining the ability of the latter enzyme to accept both PROTOGEN and COPROGEN as substrates. In the modeled tobacco PPO-substrate complex pyrrole ring A of protoporphyrinogen IX stacks against a conserved phenylalanine residue and ring B is sandwiched between two conserved leucine residues. A highly conserved arginine within the active site cavity provides a counter ion for the ring C propionate carboxylate group. Recent biochemical analysis of tobacco PPO variants showed the importance of these amino acid residues for substrate binding and catalysis.[188] In this PPO-substrate model the C20 methylene bridge of the substrate is oriented towards the

reactive N5 atom of the FAD cofactor suggesting that all hydride abstractions occur from this position. The most common mutation in human PPO causing VP is an exchange of Arg59 to tryptophane. According to the tobacco PPO structure this arginine is located on a loop between the isoalloxazine ring of FAD and the substrate-binding cavity and its replacement by a tryptophane in the human protein at this position probably disturbs the architecture of the active site and may also interfere with FAD and substrate binding.

Much less is known about the oxygen-independent PPO occurring in anaerobic bacteria and facultative anaerobes. In the mid-1970s, it was shown by Jacobs and Jacobs using cell free extracts prepared from *E. coli* that the oxygen-independent PPO activity was associated with the membrane fraction and could be solubilized by detergents. Further, it was observed that the PPO activity was coupled to the respiratory chain.[177,178,189] Later, an *E. coli* mutant strain was found which was deficient in PPO activity. The mutated gene was subsequently mapped and named *hemG*.[190,191] Only recently recombinant *E. coli* HemG was purified, characterized and shown to be an oxygen-independent PPO.[192] The protein belongs to the protein family of so-called long chain flavodoxins and contains an FMN cofactor. HemG was reported to be able to oxidize PROTOGEN to PROTO in the presence of menadione as the terminal electron acceptor substituting for the physiological, membrane-bound electron acceptor menaquinone.

Ferrochelatase

Ferrochelatase catalyzes the terminal step of heme biosynthesis, namely the insertion of ferrous iron into protoporphyrin IX. The first report describing ferrochelatase activity in avian erythrocytes was published in 1956 by Ashenbrucker *et al*. and was followed by descriptions of the same enzyme activity in a variety of cell types.[193,194] However, it took another 25 years until the first ferrochelatase was purified to homogeneity from rat liver mitochondria still with low yields.[195] In the early 1990s, the genes encoding ferrochelatase from several eukaryotic organisms were cloned and sequenced. The production of recombinant ferrochelatases finally resulted in high protein yields for functional and structural characterization. Today, ferrochelatase is one of the best characterized enzymes of the heme biosynthesis pathway.[122,194] In humans, deficiency of ferrochelatase results in the metabolic disorder erythropoietic protoporphyria (EPP). In eukaryotes ferrochelatase is a membrane-associated homodimer, while it is monomeric in bacteria.[134,186,196] In addition, in Gram-positive bacteria such as *B. subtilis* FC is a soluble protein located in the bacterial cytoplasm.[197] Eukaryotic FC proteins, with the exception of the plant enzymes, contain one [2Fe-2S] cluster per subunit.[198,199] Bacterial ferrochelatases have been described with and without FeS cluster.[200,201] However, the role of the iron-sulfur cluster is at present unknown. FC accepts a variety of different porphyrins as substrates showing that FC is rather tolerant towards different substituents on rings A and B.[122,202] In contrast the propionate side chains on rings C and D are more critical for catalysis. Some porphyrins which are not accepted as substrates like *N*-alkyl porphyrins act as competitive inhibitors.[203] FC is also able to insert divalent metal ions like Ni^{2+} and Zn^{2+} into porphyrins whereas others like Mn^{2+}, Hg^{2+}, or Pb^{2+} have inhibitory effects.[204,205] During catalysis, the planar porphyrin macrocycle has to be distorted by the enzyme into a saddle conformation to facilitate metal chelation.[136,206–208] Desolvation of ferrous iron and bond formation between the metal and two of the pyrrole nitrogens lead to a so-called "sitting-atop" complex [Fig. 5(D)]. Finally, the deprotonation of the remaining two NH-groups results in the formation of the metalated porphyrin.[207]

Although ferrochelatases from different species share little amino acid sequence identity the crystal structures of human, yeast and *B. subtilis* FC show a high degree of structural conservation. Each subunit of the dimeric eukaryotic enzymes consists of two similar domains, each containing a four-stranded parallel β-sheet surrounded by α-helices (Fig. 1). A C-terminal extension which is not present in the *B. subtilis* FC adopts a helix-turn-helix structure and is involved in coordination of the [2Fe-2S] cluster. In fact, the iron-sulfur cluster appears to contribute to anchoring the C-terminal extension to the rest of the monomer. In the FC homodimer this C-terminal extension is involved in interactions between the monomers and its absence in the *B. subtilis* enzyme might explain the monomeric structure of the latter. The active site pockets of dimeric human FC are both located on the same surface which is believed to be embedded within the membrane. The entrance of the active site pocket is lined by mostly hydrophobic residues whereas the base of the pocket is populated with several hydrophilic residues. The crystal structure of human FC in complex with PROTO revealed that the active site closes upon porphyrin binding and that the substrate is completely engulfed by the protein. Several key interactions between FC and the substrate position the porphyrin in the active site pocket [Fig. 5(C)]. The propionate carboxylate group of ring D forms a salt bridge with an arginine and that of ring C is involved in hydrogen bonding with the side chains of a serine and a tyrosine. In addition, interactions with nearby histidine and methionine, located on opposite sites of the macrocycle, also contribute to the positioning of the substrate. The FC-substrate

complex structure also revealed that PROTO is distorted by ~11.5° to adopt a modest saddle conformation which is consistent with theoretical calculations.[209] After metal insertion it was observed in a FC-product complex structure that a histidine swings away from the metallated porphyrin and that the interactions between the product ring C propionate side chain and the serine and tyrosine residues are broken. In the FC-product structure it was also observed that a structural reorganization takes place in a conserved π-helix in human FC which facilitates product release from the active site.[210] Mutations in the human ferrochelatase gene that cause EPP include missense mutations and exon deletions. Among the missense mutations which cause amino acid exchanges many lead to decreased levels of enzyme activity, although only two of them directly involve active site residues.[211]

Coordination of Heme Biosynthesis in the Cell

Several intermediates on the biosynthetic road to heme are highly unstable or reactive molecules. For example, the GluTR reaction product, GSA, is a reactive aldehyde which easily undergoes auto-cyclization or other side reactions. The linear tetrapyrrole pre-uroporphyrinogen rapidly undergoes cyclization to the non-physiological uroporphyrinogen I. Further, all porphyrinogens are easily oxidized to the corresponding porphyrins and these in turn are extremely sensitive to light, a feature exploited by photodynamic cancer therapy. As a consequence one can imagine that a highly concerted action of the heme biosynthesis enzymes is required in order to assure the efficient synthesis of this essential molecule. Such a coordinated action is achieved by (i) the co-transcription of heme biosynthesis genes and (ii) by protein-protein interactions allowing for direct product-substrate channeling between the enzymes. Indeed, the structures of GluTR and GSAM revealed a striking degree of surface complementarity and it was possible to build a model complex between the two proteins in which the active site "back door" of GluTR lies directly at the active site entrance of GSAM. In addition, complex formation between GluTR and GSAM was shown biochemically for the enzymes from *E. coli* and *C. reinhardtii*.[212,213] Therefore, the reactive GSA is directly handed over from GluTR to GSAM avoiding any contact with the aqueous medium. Complex formation was also proposed to occur between PBGD and UROS to avoid formation of uroporphyrinogen I. Although such a complex has not been shown to exist at present on the biochemical level, the genes encoding PBGD and UROS are often tandemly organized in an operon in bacteria. Finally, as for GluTR/GSAM and PBGD/UROS a direct product/substrate channeling via protein–protein interactions between PPO and ferrochelatase was proposed to occur. Indeed, it was possible to dock the structures of tobacco PPO and human FC in such a way that product/substrate channeling could take place between the two proteins.[130] In addition, it was observed that the presence of PPO is required for the iron insertion into PROTO by FC[214] and complex formation *in vivo* was shown for PPO and FC from *T. elongatus*.[215]

Conclusions

Heme is an essential molecule for all eukaryotic and most prokaryotic organisms. The enzymes involved in the multistep heme biosynthetic pathway were identified and characterized. In humans, decreased activities of these enzymes due to genetic defects are responsible for various porphyrias and X-linked sideroblastic anemia. The fact that certain enzymes are involved in heme biosynthesis exclusively in plants or bacteria makes them attractive targets for new herbicides and antimicrobial compounds. Both biochemical and structural characterization of the heme biosynthesis enzymes help to understand the molecular basis of porphyria-causing mutations and provide the means to develop new strategies for the treatment of these severe metabolic disorders as well as to design new antibiotics. Structural characterization of the enzymes proved very valuable for the current understanding of the enzyme mechanisms. In the future, additional structures of enzyme-substrate and enzyme-inhibitor complexes will certainly provide even more insight into the mechanisms of enzyme catalyzed heme biosynthesis.

Acknowledgments

The authors thank all their current and former coworkers in the field of heme biosynthesis for their invaluable contributions to the current understanding of enzyme mechanisms. Special thanks go to Prof. Wolf-Dieter Schubert (Cape Town, South Africa) and Drs. Jürgen Moser and Martina Jahn (Braunschweig, Germany) for their longstanding collaboration and work in our labs. Funding by the Deutsche Forschungsgemeinschaft and the Fonds der chemischen Industrie to G.L., D.J., and D.W.H. is gratefully acknowledged.

References

1. Munro AW, Girvan HM, McLean KJ, Cheesman MR, Leys D, Heme and hemoproteins. In: Warren MJ, Smith AG, Eds. (2009) Tetrapyrroles: birth, life and death. Austin: Landes Bioscience, pp 160–183.
2. Heinemann IU, Jahn M, Jahn D (2008) The biochemistry of heme biosynthesis. Arch Biochem Biophys 474:238–251.
3. Ajioka RS, Phillips JD, Kushner JP (2006) Biosynthesis of heme in mammals. Biochim Biophys Acta 1763: 723–736.
4. Poblete-Gutierrez P, Wiederholt T, Merk HF, Frank J (2006) The porphyrias: clinical presentation, diagnosis and treatment. Eur J Dermatol 16:230–240.

5. Battersby AR (2000) Tetrapyrroles: the pigments of life. Nat Prod Rep 17:507–526.
6. Ishida T, Yu L, Akutsu H, Ozawa K, Kawanishi S, Seto A, Inubushi T, Sano S (1998) A primitive pathway of porphyrin biosynthesis and enzymology in *Desulfovibrio vulgaris*. Proc Natl Acad Sci USA 95: 4853–4858.
7. Lobo SA, Brindley A, Warren MJ, Saraiva LM (2009) Functional characterization of the early steps of tetrapyrrole biosynthesis and modification in *Desulfovibrio vulgaris* Hildenborough. Biochem J 420:317–325.
8. Buchenau B, Kahnt J, Heinemann IU, Jahn D, Thauer RK (2006) Heme biosynthesis in *Methanosarcina barkeri* via a pathway involving two methylation reactions. J Bacteriol 188:8666–8668.
9. Jahn D, Heinz DW, Biosynthesis of 5-aminolevulinic acid. In: Warren MJ, Smith AG, Eds. (2009) Tetrapyrroles: birth, life and death. Austin: Landes Bioscience, pp 29–42.
10. Shemin D, Rittenberg D (1945) The utilization of glycine for the synthesis of a porphyrin. J Biol Chem 159:567–568.
11. Radin NS, Rittenberg D, Shemin D (1950) The role of acetic acid in the biosynthesis of heme. J Biol Chem 184:755–767.
12. Shemin D, Kumin S (1952) The mechanism of porphyrin formation: the formation of a succinyl intermediate from succinate. J Biol Chem 198:827–837.
13. Muir HM, Neuberger A (1950) The biogenesis of porphyrins. 2. The origin of the methyne carbon atoms. Biochem J 47:97–104.
14. Neuberger A, Scott JJ (1953) Aminolaevulinic acid and porphyrin biosynthesis. Nature 172:1093–1094.
15. Shemin D, Russell CS (1953) Aminolevulinic acid, its role in the biosynthesis of porphyrins and purines. J Am Chem Soc 75:4873–4874.
16. Kikuchi G, Kumar A, Talmage P, Shemin D (1958) The enzymatic synthesis of delta-aminolevulinic acid. J Biol Chem 233:1214–1219.
17. Kikuchi G, Shemin D, Bachmann BJ (1958) The enzymic synthesis of delta-aminolevulinic acid. Biochim Biophys Acta 28:219–220.
18. Gibson KD, Laver WG, Neuberger A (1958) Initial stages in the biosynthesis of porphyrins. 2. The formation of delta-aminolaevulic acid from glycine and succinyl-coenzyme A by particles from chicken erythrocytes. Biochem J 70:71–81.
19. Laver WG, Neuberger A, Udenfriend S (1958) Initial stages in the biosynthesis of porphyrins. I. The formation of delta-aminolaevulic acid by particles obtained from chicken erythrocytes. Biochem J 70:4–14.
20. Ferreira GC, Gong J (1995) 5-Aminolevulinate synthase and the first step of heme biosynthesis. J Bioenerg Biomembr 27:151–159.
21. Bishop DF, Henderson AS, Astrin KH (1990) Human delta-aminolevulinate synthase: assignment of the housekeeping gene to 3p21 and the erythroid-specific gene to the X chromosome. Genomics 7:207–214.
22. Camaschella C (2008) Recent advances in the understanding of inherited sideroblastic anaemia. Br J Haematol 143:27–38.
23. Whatley SD, Ducamp S, Gouya L, Grandchamp B, Beaumont C, Badminton MN, Elder GH, Holme SA, Anstey AV, Parker M (2008) C-terminal deletions in the ALAS2 gene lead to gain of function and cause X-linked dominant protoporphyria without anemia or iron overload. Am J Hum Genet 83:408–414.
24. Astner I, Schulze JO, van den Heuvel J, Jahn D, Schubert WD, Heinz DW (2005) Crystal structure of 5-aminolevulinate synthase, the first enzyme of heme biosynthesis, and its link to XLSA in humans. Embo J 24:3166–3177.
25. Fanica-Gaignier M, Clement-Metral J (1973) 5-Aminolevulinic-acid synthetase of *Rhodopseudomonas spheroides* Y. Purification and some properties. Eur J Biochem 40:13–18.
26. Nandi DL (1978) Delta-aminolevulinic acid synthase of *Rhodopseudomonas spheroides*. Binding of pyridoxal phosphate to the enzyme. Arch Biochem Biophys 188:266–271.
27. Alexander FW, Sandmeier E, Mehta PK, Christen P (1994) Evolutionary relationships among pyridoxal-5′-phosphate-dependent enzymes. Regio-specific alpha, beta and gamma families. Eur J Biochem 219: 953–960.
28. Akhtar M, Jordan PM (1968) The mechanism of the action of delta-aminolaevulate synthetase and the synthesis of stereospecifically tritiated glycine. J Chem Soc Chem Commun 1691–1692.
29. Zaman Z, Jordan PM, Akhtar M (1973) Mechanism and stereochemistry of the 5-aminolaevulinate synthetase reaction. Biochem J 135:257–263.
30. Abboud MM, Jordan PM, Akhtar M (1974) Biosynthesis of 5-aminolevulinic acid: involvement of a retention–inversion mechanism. J Chem Soc Chem Commun 643–644.
31. Hunter GA, Ferreira GC (1995) A continuous spectrophotometric assay for 5-aminolevulinate synthase that utilizes substrate cycling. Anal Biochem 226: 221–224.
32. Hunter GA, Ferreira GC (1999) Lysine-313 of 5-aminolevulinate synthase acts as a general base during formation of the quinonoid reaction intermediates. Biochemistry 38:3711–3718.
33. Hunter GA, Ferreira GC (1999) Pre-steady-state reaction of 5-aminolevulinate synthase. Evidence for a rate-determining product release. J Biol Chem 274: 12222–12228.
34. Hunter GA, Zhang J, Ferreira GC (2007) Transient kinetic studies support refinements to the chemical and kinetic mechanisms of aminolevulinate synthase. J Biol Chem 282:23025–23035.
35. Hunter GA, Ferreira GC (2009) 5-Aminolevulinate synthase: catalysis of the first step of heme biosynthesis. Cell Mol Biol (Noisy-le-grand) 55:102–110.
36. Beale SI, Castelfranco PA (1973) 14C incorporation from exogenous compounds into delta-aminolevulinic acid by greening cucumber cotyledons. Biochem Biophys Res Commun 52:143–149.
37. Beale SI, Gough SP, Granick S (1975) Biosynthesis of delta-aminolevulinic acid from the intact carbon skeleton of glutamic acid in greening barley. Proc Natl Acad Sci USA 72:2719–2723.
38. Kannangara CG, Gough SP (1978) Biosynthesis of delta-aminolevulinate in greening barley leaves: glutamate-1-semialdehyde aminotransferase. Carlsberg Res Commun 43:185–194.
39. Kannangara CG, Gough SP, Girnth CR, Delta-aminolevulinate synthesis in greening barley. 2. Purification of enzymes. In: Akoyunoglou G, Ed. (1981) Proceedings of Fifth International Congress in Photosynthesis. Volume 5. Philadelphia: Balaban Int Sci Ser, pp 117–127.
40. Huang DD, Wang WY, Gough SP, Kannangara CG (1984) Delta-aminolevulinic acid synthesizing enzymes need an RNA moiety for activity. Science 225:1482–1484.
41. Kannangara CG, Gough SP, Bruyant P, Hoober JK, Kahn A, von Wettstein D (1988) tRNA(Glu) as a

cofactor in delta-aminolevulinate biosynthesis: steps that regulate chlorophyll synthesis. Trends Biochem Sci 13:139–143.
42. Jahn D, Verkamp E, Soll D (1992) Glutamyl-transfer RNA: a precursor of heme and chlorophyll biosynthesis. Trends Biochem Sci 17:215–218.
43. Chen MW, Jahn D, O'Neill GP, Soll D (1990) Purification of the glutamyl-tRNA reductase from *Chlamydomonas reinhardtii* involved in delta-aminolevulinic acid formation during chlorophyll biosynthesis. J Biol Chem 265:4058–4063.
44. Rieble S, Beale SI (1991) Purification of glutamyl-tRNA reductase from *Synechocystis* sp. PCC 6803. J Biol Chem 266:9740–9745.
45. Pontoppidan B, Kannangara CG (1994) Purification and partial characterization of barley glutamyl-tRNA(Glu) reductase, the enzyme that directs glutamate to chlorophyll biosynthesis. Eur J Biochem 225: 529–537.
46. Moser J, Lorenz S, Hubschwerlen C, Rompf A, Jahn D (1999) *Methanopyrus kandleri* glutamyl-tRNA reductase. J Biol Chem 274:30679–30685.
47. Wang WY, Huang DD, Stachon D, Gough SP, Kannangara CG (1984) Purification, characterization, and fractionation of the delta-aminolevulinic acid synthesizing enzymes from light-grown *Chlamydomonas reinhardtii* cells. Plant Physiol 74:569–575.
48. Hoober JK, Kahn A, Ash DE, Gough S, Kannangara CG (1988) Biosynthesis of delta-aminolevulinate in greening barley leaves. IX. Structure of the substrate, mode of gabaculine inhibition, and the catalytic mechanism of glutamate 1-semialdehyde aminotransferase. Carlsberg Res Commun 53:11–25.
49. Grimm B (1990) Primary structure of a key enzyme in plant tetrapyrrole synthesis: glutamate 1-semialdehyde aminotransferase. Proc Natl Acad Sci USA 87: 4169–4173.
50. Jahn D, Chen MW, Soll D (1991) Purification and functional characterization of glutamate-1-semialdehyde aminotransferase from *Chlamydomonas reinhardtii*. J Biol Chem 266:161–167.
51. Smith MA, Grimm B, Kannangara CG, von Wettstein D (1991) Spectral kinetics of glutamate-1-semialdehyde aminomutase of *Synechococcus*. Proc Natl Acad Sci USA 88:9775–9779.
52. Palmieri G, Di Palo M, Scaloni A, Orru S, Marino G, Sannia G (1996) Glutamate-1-semialdehyde aminotransferase from *Sulfolobus solfataricus*. Biochem J 320 (Part 2):541–545.
53. Moser J, Schubert WD, Beier V, Bringemeier I, Jahn D, Heinz DW (2001) V-shaped structure of glutamyl-tRNA reductase, the first enzyme of tRNA-dependent tetrapyrrole biosynthesis. Embo J 20:6583–6590.
54. Hennig M, Grimm B, Contestabile R, John RA, Jansonius JN (1997) Crystal structure of glutamate-1-semialdehyde aminomutase: an alpha2-dimeric vitamin B6-dependent enzyme with asymmetry in structure and active site reactivity. Proc Natl Acad Sci USA 94: 4866–4871.
55. Schulze JO, Schubert WD, Moser J, Jahn D, Heinz DW (2006) Evolutionary relationship between initial enzymes of tetrapyrrole biosynthesis. J Mol Biol 358: 1212–1220.
56. Randau L, Schauer S, Ambrogelly A, Salazar JC, Moser J, Sekine S, Yokoyama S, Soll D, Jahn D (2004) tRNA recognition by glutamyl-tRNA reductase. J Biol Chem 279:34931–34937.
57. Luer C, Schauer S, Virus S, Schubert WD, Heinz DW, Moser J, Jahn D (2007) Glutamate recognition and hydride transfer by *Escherichia coli* glutamyl-tRNA reductase. Febs J 274:4609–4614.
58. Schauer S, Chaturvedi S, Randau L, Moser J, Kitabatake M, Lorenz S, Verkamp E, Schubert WD, Nakayashiki T, Murai M (2002) *Escherichia coli* glutamyl-tRNA reductase. Trapping the thioester intermediate. J Biol Chem 277:48657–48663.
59. Grimm B, Smith MA, von Wettstein D (1992) The role of Lys272 in the pyridoxal 5-phosphate active site of *Synechococcus* glutamate-1-semialdehyde aminotransferase. Eur J Biochem 206:579–585.
60. Tyacke RJ, Harwood JL, John RA (1993) Properties of the pyridoxaldimine form of glutamate semialdehyde aminotransferase (glutamate-1-semialdehyde 2,1-aminomutase) and analysis of its role as an intermediate in the formation of aminolaevulinate. Biochem J 293 (Part 3):697–701.
61. Brody S, Andersen JS, Kannangara CG, Meldgaard M, Roepstorff P, von Wettstein D (1995) Characterization of the different spectral forms of glutamate 1-semialdehyde aminotransferase by mass spectrometry. Biochemistry 34:15918–15924.
62. Ilag LL, Jahn D (1992) Activity and spectroscopic properties of the *Escherichia coli* glutamate 1-semialdehyde aminotransferase and the putative active site mutant K265R. Biochemistry 31:7143–7151.
63. Pugh CE, Harwood JL, John RA (1992) Mechanism of glutamate semialdehyde aminotransferase. Roles of diamino- and dioxo-intermediates in the synthesis of aminolevulinate. J Biol Chem 267:1584–1588.
64. Friedmann HC, Duban ME, Valasinas A, Frydman B (1992) The enantioselective participation of (S)- and (R)-diaminovaleric acids in the formation of delta-aminolevulinic acid in cyanobacteria. Biochem Biophys Res Commun 185:60–68.
65. Smith MA, King PJ, Grimm B (1998) Transient-state kinetic analysis of *Synechococcus* glutamate 1-semialdehyde aminotransferase. Biochemistry 37:319–329.
66. Orriss GL, Patel TR, Sorensen J, Stetefeld J (2010) Absence of a catalytic water confers resistance to the neurotoxin gabaculine. Faseb J 24:404–414.
67. Sachs P (1931) Ein Fall von akuter Porphyrie mit hochgradiger Muskelatropie. Klin Wschr 10:1123–1125.
68. Westall RG (1952) Isolation of porphobilinogen from the urine of a patient with acute porphyria. Nature 170:614–616.
69. Cookson GH, Rimington C (1953) Porphobilinogen: chemical constitution. Nature 171:875–876.
70. Falk JE, Dresel EI, Rimington C (1953) Porphobilinogen as a porphyrin precursor, and interconversion of porphyrins, in a tissue system. Nature 172:292–294.
71. Gibson KD, Neuberger A, Scott JJ (1954) The enzymic conversion of delta-aminolaevulic acid to porphobilinogen. Biochem J 58:xli–xlii.
72. Schmid R, Shemin D (1955) The enzymatic formation of porphobilinogen from delta-aminolevulinic acid and its conversion to protoporphyrin. J Am Chem Soc 77: 506–507.
73. Bogorad L, Granick S (1953) The enzymatic synthesis of porphyrins from porphobilinogen. Proc Natl Acad Sci USA 39:1176–1188.
74. Bogorad L (1958) The enzymatic synthesis of porphyrins from porphobilinogen. II. Uroporphyrin III. J Biol Chem 233:510–515.
75. Neve RA, Labbe RF, Aldrich RA (1956) Reduced uroporphyrin III in the biosynthesis of heme. J Am Chem Soc 78:691–692.
76. Schubert HL, Erskine PT, Cooper JB, 5-Aminolevulinic acid dehydratase, porphobilinogen deaminase

and uroporphyrinogen III synthase. In: Warren MJ, Smith AG, Eds. (2009) Tetrapyrroles: birth, life and death. Austin: Landes Bioscience, pp 43–73.
77. Erskine PT, Senior N, Awan S, Lambert R, Lewis G, Tickle IJ, Sarwar M, Spencer P, Thomas P, Warren MJ (1997) X-ray structure of 5-aminolaevulinate dehydratase, a hybrid aldolase. Nat Struct Biol 4: 1025–1031.
78. Erskine PT, Norton E, Cooper JB, Lambert R, Coker A, Lewis G, Spencer P, Sarwar M, Wood SP, Warren MJ (1999) X-ray structure of 5-aminolevulinic acid dehydratase from *Escherichia coli* complexed with the inhibitor levulinic acid at 2.0 A resolution. Biochemistry 38:4266–4276.
79. Frankenberg N, Erskine PT, Cooper JB, Shoolingin-Jordan PM, Jahn D, Heinz DW (1999) High resolution crystal structure of a Mg2+-dependent porphobilinogen synthase. J Mol Biol 289:591–602.
80. Coates L, Beaven G, Erskine PT, Beale SI, Avissar YJ, Gill R, Mohammed F, Wood SP, Shoolingin-Jordan P, Cooper JB (2004) The X-ray structure of the plant like 5-aminolaevulinic acid dehydratase from *Chlorobium vibrioforme* complexed with the inhibitor laevulinic acid at 2.6 A resolution. J Mol Biol 342:563–570.
81. Louie GV, Brownlie PD, Lambert R, Cooper JB, Blundell TL, Wood SP, Warren MJ, Woodcock SC, Jordan PM (1992) Structure of porphobilinogen deaminase reveals a flexible multidomain polymerase with a single catalytic site. Nature 359:33–39.
82. Song G, Li Y, Cheng C, Zhao Y, Gao A, Zhang R, Joachimiak A, Shaw N, Liu ZJ (2009) Structural insight into acute intermittent porphyria. Faseb J 23: 396–404.
83. Gill R, Kolstoe SE, Mohammed F, Al DBA, Mosely JE, Sarwar M, Cooper JB, Wood SP, Shoolingin-Jordan PM (2009) Structure of human porphobilinogen deaminase at 2.8 A: the molecular basis of acute intermittent porphyria. Biochem J 420:17–25.
84. Mathews MA, Schubert HL, Whitby FG, Alexander KJ, Schadick K, Bergonia HA, Phillips JD, Hill CP (2001) Crystal structure of human uroporphyrinogen III synthase. Embo J 20:5832–5839.
85. Schubert HL, Phillips JD, Heroux A, Hill CP (2008) Structure and mechanistic implications of a uroporphyrinogen III synthase-product complex. Biochemistry 47:8648–8655.
86. Bollivar DW, Clauson C, Lighthall R, Forbes S, Kokona B, Fairman R, Kundrat L, Jaffe EK (2004) *Rhodobacter capsulatus* porphobilinogen synthase, a high activity metal ion independent hexamer. BMC Biochem 5:17.
87. Jaffe EK (2004) The porphobilinogen synthase catalyzed reaction mechanism. Bioorg Chem 32:316–325.
88. Chaudhry AG, Jordan PM (1976) Stereochemical studies on the formation of porphobilinogen. Biochem Soc Trans 4:760–761.
89. Jordan PM, Gibbs PN (1985) Mechanism of action of 5-aminolaevulinate dehydratase from human erythrocytes. Biochem J 227:1015–1020.
90. Erskine PT, Coates L, Newbold R, Brindley AA, Stauffer F, Wood SP, Warren MJ, Cooper JB, Shoolingin-Jordan PM, Neier R (2001) The X-ray structure of yeast 5-aminolaevulinic acid dehydratase complexed with two diacid inhibitors. FEBS Lett 503:196–200.
91. Kervinen J, Jaffe EK, Stauffer F, Neier R, Wlodawer A, Zdanov A (2001) Mechanistic basis for suicide inactivation of porphobilinogen synthase by 4,7-dioxosebacic acid, an inhibitor that shows dramatic species selectivity. Biochemistry 40:8227–8236.
92. Jaffe EK, Kervinen J, Martins J, Stauffer F, Neier R, Wlodawer A, Zdanov A (2002) Species-specific inhibition of porphobilinogen synthase by 4-oxosebacic acid. J Biol Chem 277:19792–19799.
93. Frere F, Schubert WD, Stauffer F, Frankenberg N, Neier R, Jahn D, Heinz DW (2002) Structure of porphobilinogen synthase from *Pseudomonas aeruginosa* in complex with 5-fluorolevulinic acid suggests a double Schiff base mechanism. J Mol Biol 320:237–247.
94. Erskine PT, Coates L, Butler D, Youell JH, Brindley AA, Wood SP, Warren MJ, Shoolingin-Jordan PM, Cooper JB (2003) X-ray structure of a putative reaction intermediate of 5-aminolaevulinic acid dehydratase. Biochem J 373:733–738.
95. Goodwin CE, Leeper FJ (2003) Stereochemistry and mechanism of the conversion of 5-aminolaevulinic acid into porphobilinogen catalysed by porphobilinogen synthase. Org Biomol Chem 1:1443–1446.
96. Frere F, Nentwich M, Gacond S, Heinz DW, Neier R, Frankenberg-Dinkel N (2006) Probing the active site of *Pseudomonas aeruginosa* porphobilinogen synthase using newly developed inhibitors. Biochemistry 45: 8243–8253.
97. Breinig S, Kervinen J, Stith L, Wasson AS, Fairman R, Wlodawer A, Zdanov A, Jaffe EK (2003) Control of tetrapyrrole biosynthesis by alternate quaternary forms of porphobilinogen synthase. Nat Struct Biol 10:757–763.
98. Heinemann IU, Schulz C, Schubert WD, Heinz DW, Wang YG, Kobayashi Y, Awa Y, Wachi M, Jahn D, Jahn M (2009) Structure of the heme biosynthetic *Pseudomonas aeruginosa* porphobilinogen synthase in complex with the antibiotic alaremycin. Antimicrob Agents Chemother 54:267–272.
99. Battersby AR, Hodgson GL, Hunt E, McDonald E, Saunders J (1976) Biosynthesis of porphyrins and related macrocycles. Part VI. Nature of the rearrangement process leading to the natural type III porphyrins. J Chem Soc Perkin Trans 1:273–282.
100. Battersby AR, Fookes CJR, Meegan MJ, McDonald E, Wurziger HKW (1981) Biosynthesis of porphyrins and related macrocycles. Part 16. Proof that the single intramolecular rearrangement leading to natural porphyrins (type-III) occurs at the tetrapyrrole level. J Chem Soc Perkin Trans 1:2786–2799.
101. Battersby AR, Fookes CJR, Matcham GWJ, McDonald E (1979) Order of assembly of the four pyrrole rings during biosynthesis of the natural porphyrins. J Chem Soc Chem Commun 539–541.
102. Jordan PM, Seehra JS (1979) The biosynthesis of uroporphyrinogen III: order of assembly of the four porphobilinogen molecules in the formation of the tetrapyrrole ring. FEBS Lett 104:364–366.
103. Burton G, Fagerness PE, Hosozawa S, Jordan PM, Scott AI (1979) 13C NMR evidence for a new intermediate, pre-uroporphyrinogen, in the enzymic transformation of porphobilinogen into uroporphyrinogens I and III. J Chem Soc Chem Commun 202–204.
104. Battersby AR, Fookes CJR, Gustafson-Potter KE, McDonald E, Matcham GWJ (1979) Biosynthesis of the natural porphyrins: experiments on the ring-closure steps and with the hydroxy-analogue of porphobilinogen. J Chem Soc Chem Commun 316–319.
105. Battersby AR, Fookes CJR, Gustafson-Potter KE, McDonald E, Matcham GWJ (1982) Biosynthesis of porphyrins and related macrocycles. Part 18. Proof by spectroscopy and synthesis that unrearranged hydroxymethylbilane is the product from deaminase and the substrate for cosynthetase in the biosynthesis of

uroporphyrinogen-III. J Chem Soc Perkin Trans 1: 2427–2444.
106. Hart GJ, Miller AD, Leeper FJ, Battersby AR (1987) Biosynthesis of the natural porphyrins: proof that hydroxymethylbilane synthase (porphobilinogen deaminase) uses a novel binding group in its catalytic action. J Chem Soc Chem Commun 1762–1765.
107. Jordan PM, Warren MJ (1987) Evidence for a dipyrromethane cofactor at the catalytic site of *E. coli* porphobilinogen deaminase. FEBS Lett 225:87–92.
108. Warren MJ, Jordan PM (1988) Investigation into the nature of substrate binding to the dipyrromethane cofactor of *Escherichia coli* porphobilinogen deaminase. Biochemistry 27:9020–9030.
109. Warren MJ, Scott AI (1990) Tetrapyrrole assembly and modification into the ligands of biologically functional cofactors. Trends Biochem Sci 15:486–491.
110. Woodcock SC, Jordan PM (1994) Evidence for participation of aspartate-84 as a catalytic group at the active site of porphobilinogen deaminase obtained by site-directed mutagenesis of the *hemC* gene from *Escherichia coli*. Biochemistry 33:2688–2695.
111. Warren MJ, Gul S, Aplin RT, Scott AI, Roessner CA, O'Grady P, Shoolingin-Jordan PM (1995) Evidence for conformational changes in *Escherichia coli* porphobilinogen deaminase during stepwise pyrrole chain elongation monitored by increased reactivity of cysteine-134 to alkylation by N-ethylmaleimide. Biochemistry 34:11288–11295.
112. Mathewson JH, Corwin AH (1961) Biosynthesis of pyrrole pigments: a mechanism for porphobilinogen polymerization. J Am Chem Soc 83:135–137.
113. Shoolingin-Jordan PM (1995) Porphobilinogen deaminase and uroporphyrinogen III synthase: structure, molecular biology, and mechanism. J Bioenerg Biomembr 27:181–195.
114. Spivey AC, Capretta A, Frampton CS, Leeper FJ, Battersby AR (1996) Biosynthesis of porphyrins and related macrocycles. Part 45. Determination by a novel X-ray method of the absolute configuration of the spiro lactam which inhibits uroporphyrinogen III synthase (cosynthetase). J Chem Soc Perkin Trans 1:2091–2102.
115. Silva PJ, Ramos MJ (2008) Comparative density functional study of models for the reaction mechanism of uroporphyrinogen III synthase. J Phys Chem B 112: 3144–3148.
116. Battersby AR, Fookes CJR, Pandey PS (1983) Linear tetrapyrrolic intermediates for biosynthesis of the natural porphyrins. Experiments with modified substrates. Tetrahedron 39:1919–1926.
117. Pichon C, Atshaves BP, Xue T, Stolowich NJ, Scott AI (1994) Studies on uro'gen III synthase with modified bilanes. Bioorg Med Chem 4:1105–1110.
118. Tan FC, Cheng Q, Saha K, Heinemann IU, Jahn M, Jahn D, Smith AG (2008) Identification and characterization of the *Arabidopsis* gene encoding the tetrapyrrole biosynthesis enzyme uroporphyrinogen III synthase. Biochem J 410:291–299.
119. Cornah JE, Smith AG, Transformation of uroporphyrinogen III into protohaem. In: Warren MJ, Smith AG, Eds. (2009) Tetrapyrroles: birth, life and death. Austin: Landes Bioscience, pp 74–88.
120. Shoolingin-Jordan PM, The biosynthesis of coproporphyrinogen III. In: Kadish KM, Smith KM, Guilard R, Eds. (2003) The porphyrin handbook, Vol. 12, The iron and cobalt pigments: biosynthesis, structure and degradation. New York: Elsevier, pp 33–74.
121. Akhtar M, Coproporphyrinogen III and protoporphyrinogen IX oxidases. In: Kadish KM, Smith KM, Guilard R, Eds. (2003) The porphyrin handbook, Vol. 12, The iron and cobalt pigments: biosynthesis, structure and degradation. New York: Elsevier, pp 75–92.
122. Dailey H, Dailey T, Ferrochelatase. In: Kadish KM, Smith KM, Guilard R, Eds. (2003) The porphyrin handbook, Vol. 12, The iron and cobalt pigments: biosynthesis, structure and degradation. New York: Elsevier, pp 93–121.
123. Whitby FG, Phillips JD, Kushner JP, Hill CP (1998) Crystal structure of human uroporphyrinogen decarboxylase. Embo J 17:2463–2471.
124. Phillips JD, Whitby FG, Kushner JP, Hill CP (2003) Structural basis for tetrapyrrole coordination by uroporphyrinogen decarboxylase. Embo J 22:6225–6233.
125. Martins BM, Grimm B, Mock HP, Huber R, Messerschmidt A (2001) Crystal structure and substrate binding modeling of the uroporphyrinogen-III decarboxylase from *Nicotiana tabacum*. Implications for the catalytic mechanism. J Biol Chem 276:44108–44116.
126. Fan J, Liu Q, Hao Q, Teng M, Niu L (2007) Crystal structure of uroporphyrinogen decarboxylase from *Bacillus subtilis*. J Bacteriol 189:3573–3580.
127. Phillips JD, Whitby FG, Warby CA, Labbe P, Yang C, Pflugrath JW, Ferrara JD, Robinson H, Kushner JP, Hill CP (2004) Crystal structure of the oxygen-dependent coproporphyrinogen oxidase (Hem13p) of *Saccharomyces cerevisiae*. J Biol Chem 279:38960–38968.
128. Lee DS, Flachsova E, Bodnarova M, Demeler B, Martasek P, Raman CS (2005) Structural basis of hereditary coproporphyria. Proc Natl Acad Sci USA 102: 14232–14237.
129. Layer G, Moser J, Heinz DW, Jahn D, Schubert WD (2003) Crystal structure of coproporphyrinogen III oxidase reveals cofactor geometry of Radical SAM enzymes. Embo J 22:6214–6224.
130. Koch M, Breithaupt C, Kiefersauer R, Freigang J, Huber R, Messerschmidt A (2004) Crystal structure of protoporphyrinogen IX oxidase: a key enzyme in haem and chlorophyll biosynthesis. Embo J 23:1720–1728.
131. Corradi HR, Corrigall AV, Boix E, Mohan CG, Sturrock ED, Meissner PN, Acharya KR (2006) Crystal structure of protoporphyrinogen oxidase from *Myxococcus xanthus* and its complex with the inhibitor acifluorfen. J Biol Chem 281:38625–38633.
132. Qin X, Sun L, Wen X, Yang X, Tan Y, Jin H, Cao Q, Zhou W, Xi Z, Shen Y (2010) Structural insight into unique properties of protoporphyrinogen oxidase from *Bacillus subtilis*. J Struct Biol 170:76–82.
133. Al-Karadaghi S, Hansson M, Nikonov S, Jonsson B, Hederstedt L (1997) Crystal structure of ferrochelatase: the terminal enzyme in heme biosynthesis. Structure 5:1501–1510.
134. Wu CK, Dailey HA, Rose JP, Burden A, Sellers VM, Wang BC (2001) The 2.0 A structure of human ferrochelatase, the terminal enzyme of heme biosynthesis. Nat Struct Biol 8:156–160.
135. Karlberg T, Lecerof D, Gora M, Silvegren G, Labbe-Bois R, Hansson M, Al-Karadaghi S (2002) Metal binding to *Saccharomyces cerevisiae* ferrochelatase. Biochemistry 41:13499–13506.
136. Medlock A, Swartz L, Dailey TA, Dailey HA, Lanzilotta WN (2007) Substrate interactions with human ferrochelatase. Proc Natl Acad Sci USA 104:1789–1793.
137. Mauzerall D, Granick S (1958) Porphyrin biosynthesis in erythrocytes. III. Uroporphyrinogen and its decarboxylase. J Biol Chem 232:1141–1162.
138. Jackson AH, Sancovich HA, Ferramola AM, Evans N, Games DE, Matlin SA, Elder GH, Smith SG (1976)

Macrocyclic intermediates in the biosynthesis of porphyrins. Philos Trans R Soc Lond B Biol Sci 273: 191–206.
139. Lim CK, Rideout JM, Wright DJ (1983) High-performance liquid chromatography of naturally occurring 8-, 7-, 6-, 5- and 4-carboxylic porphyrin isomers. J Chromatogr 282:629–641.
140. Akhtar M, Mechanism and stereochemistry of the enzymes involved in the conversion of uroporphyrinogen III into haem. In: Jordan PM, Ed. (1991) New comprehensive biochemistry, Vol. 19, Biosynthesis of tetrapyrroles. Amsterdam: Elsevier, pp 67–99.
141. Smith AG, Francis JE (1979) Decarboxylation of porphyrinogens by rat liver uroporphyrinogen decarboxylase. Biochem J 183:455–458.
142. Luo J, Lim CK (1993) Order of uroporphyrinogen III decarboxylation on incubation of porphobilinogen and uroporphyrinogen III with erythrocyte uroporphyrinogen decarboxylase. Biochem J 289 (Part 2):529–532.
143. Lewis CA, Jr, Wolfenden R (2008) Uroporphyrinogen decarboxylation as a benchmark for the catalytic proficiency of enzymes. Proc Natl Acad Sci USA 105: 17328–17333.
144. Phillips JD, Warby CA, Whitby FG, Kushner JP, Hill CP (2009) Substrate shuttling between active sites of uroporphyrinogen decarboxylase is not required to generate coproporphyrinogen. J Mol Biol 389:306–314.
145. Cavallaro G, Decaria L, Rosato A (2008) Genome-based analysis of heme biosynthesis and uptake in prokaryotic systems. J Proteome Res 7:4946–4954.
146. Martasek P (1998) Hereditary coproporphyria. Semin Liver Dis 18:25–32.
147. Sano S, Granick S (1961) Mitochondrial coproporphyrinogen oxidase and protoporphyrin formation. J Biol Chem 236:1173–1180.
148. del Batlle AM, Benson A, Rimington C (1965) Purification and properties of coproporphyrinogenase. Biochem J 97:731–740.
149. Poulson R, Polglase WJ (1974) Aerobic and anaerobic coproporphyrinogenase activities in extracts from *Saccharomyces cerevisiae*. J Biol Chem 249:6367–6371.
150. Yoshinaga T, Sano S (1980) Coproporphyrinogen oxidase. II. Reaction mechanism and role of tyrosine residues on the activity. J Biol Chem 255:4727–4731.
151. Yoshinaga T, Sano S (1980) Coproporphyrinogen oxidase. I. Purification, properties, and activation by phospholipids. J Biol Chem 255:4722–4726.
152. Labbe P (1997) Purification and properties of coproporphyrinogen III oxidase from yeast. Methods Enzymol 281:367–378.
153. Kohno H, Furukawa T, Tokunaga R, Taketani S, Yoshinaga T (1996) Mouse coproporphyrinogen oxidase is a copper-containing enzyme: expression in *Escherichia coli* and site-directed mutagenesis. Biochim Biophys Acta 1292:156–162.
154. Medlock AE, Dailey HA (1996) Human coproporphyrinogen oxidase is not a metalloprotein. J Biol Chem 271:32507–32510.
155. Breckau D, Mahlitz E, Sauerwald A, Layer G, Jahn D (2003) Oxygen-dependent coproporphyrinogen III oxidase (HemF) from *Escherichia coli* is stimulated by manganese. J Biol Chem 278:46625–46631.
156. Cavaleiro JAS, Kenner GW, Smith KM (1974) Pyrroles and related compounds. Part XXXII. Biosynthesis of protoporphyrin-IX from coproporphyrinogen-III. J Chem Soc Perkin Trans 1:1188–1194.
157. Elder GH, Evans JO, Jackson JR, Jackson AH (1978) Factors determining the sequence of oxidative decarboxylation of the 2- and 4-propionate substituents of coproporphyrinogen III by coproporphyrinogen oxidase in rat liver. Biochem J 169:215–223.
158. Zaman Z, Akhtar M (1976) Mechanism and stereochemistry of vinyl-group formation in haem biosynthesis. Eur J Biochem 61:215–223.
159. Seehra JS, Jordan PM, Akhtar M (1983) Anaerobic and aerobic coproporphyrinogen III oxidases of *Rhodopseudomonas spheroides*. Mechanism and stereochemistry of vinyl group formation. Biochem J 209:709–718.
160. Battersby AR, McDonald E, Wurziger HKW, James KJ (1975) Stereochemistry of biosynthesis of the vinyl groups of protoporphyrin-IX: a short synthesis of porphobilinogen. J Chem Soc Chem Commun 493–494.
161. Lash TD (2005) The enigma of coproporphyrinogen oxidase: how does this unusual enzyme carry out oxidative decarboxylations to afford vinyl groups? Bioorg Med Chem Lett 15:4506–4509.
162. Silva PJ, Ramos MJ (2008) A comparative density-functional study of the reaction mechanism of the O2-dependent coproporphyrinogen III oxidase. Bioorg Med Chem 16:2726–2733.
163. Stephenson JR, Stacey JA, Morgenthaler JB, Friesen JA, Lash TD, Jones MA (2007) Role of aspartate 400, arginine 262, and arginine 401 in the catalytic mechanism of human coproporphyrinogen oxidase. Protein Sci 16:401–410.
164. Tait GH (1969) Coproporphyrinogenase activity in extracts from *Rhodopseudomonas spheroides*. Biochem Biophys Res Commun 37:116–122.
165. Tait GH (1972) Coproporphyrinogenase activities in extracts of *Rhodopseudomonas spheroides* and *Chromatium* strain D. Biochem J 128:1159–1169.
166. Coomber SA, Jones RM, Jordan PM, Hunter CN (1992) A putative anaerobic coproporphyrinogen III oxidase in *Rhodobacter sphaeroides*. I. Molecular cloning, transposon mutagenesis and sequence analysis of the gene. Mol Microbiol 6:3159–3169.
167. Xu K, Elliott T (1994) Cloning, DNA sequence, and complementation analysis of the *Salmonella typhimurium hemN* gene encoding a putative oxygen-independent coproporphyrinogen III oxidase. J Bacteriol 176:3196–3203.
168. Troup B, Hungerer C, Jahn D (1995) Cloning and characterization of the *Escherichia coli hemN* gene encoding the oxygen-independent coproporphyrinogen III oxidase. J Bacteriol 177:3326–3331.
169. Lieb C, Siddiqui RA, Hippler B, Jahn D, Friedrich B (1998) The *Alcaligenes eutrophus hemN* gene encoding the oxygen-independent coproporphyrinogen III oxidase, is required for heme biosynthesis during anaerobic growth. Arch Microbiol 169:52–60.
170. Fischer HM, Velasco L, Delgado MJ, Bedmar EJ, Scharen S, Zingg D, Gottfert M, Hennecke H (2001) One of two *hemN* genes in *Bradyrhizobium japonicum* is functional during anaerobic growth and in symbiosis. J Bacteriol 183:1300–1311.
171. Layer G, Verfurth K, Mahlitz E, Jahn D (2002) Oxygen-independent coproporphyrinogen-III oxidase HemN from *Escherichia coli*. J Biol Chem 277: 34136–34142.
172. Layer G, Pierik AJ, Trost M, Rigby SE, Leech HK, Grage K, Breckau D, Astner I, Jansch L, Heathcote P (2006) The substrate radical of *Escherichia coli* oxygen-independent coproporphyrinogen III oxidase HemN. J Biol Chem 281:15727–15734.
173. Layer G, Grage K, Teschner T, Schunemann V, Breckau D, Masoumi A, Jahn M, Heathcote P, Trautwein AX, Jahn D (2005) Radical S-adenosylmethionine enzyme

coproporphyrinogen III oxidase HemN: functional features of the [4Fe-4S] cluster and the two bound S-adenosyl-L-methionines. J Biol Chem 280:29038–29046.
174. Rand K, Noll C, Schiebel HM, Kemken D, Dulcks T, Kalesse M, Heinz DW, Layer G (2010) The oxygen-independent coproporphyrinogen III oxidase HemN utilizes harderoporphyrinogen as a reaction intermediate during conversion of coproporphyrinogen III to protoporphyrinogen IX. Biol Chem 391:55–63.
175. Porra RJ, Falk JE (1961) Protein-bound porphyrins associated with protoporphyrin biosynthesis. Biochem Biophys Res Commun 5:179–184.
176. Porra RJ, Falk JE (1964) The enzymic conversion of coproporphyrinogen 3 into protoporphyrin 9. Biochem J 90:69–75.
177. Jacobs NJ, Jacobs JM (1975) Fumarate as alternate electron acceptor for the late steps of anaerobic heme synthesis in *Escherichia coli*. Biochem Biophys Res Commun 65:435–441.
178. Jacobs NJ, Jacobs JM (1976) Nitrate, fumarate, and oxygen as electron acceptors for a late step in microbial heme synthesis. Biochim Biophys Acta 449:1–9.
179. Siepker LJ, Ford M, de Kock R, Kramer S (1987) Purification of bovine protoporphyrinogen oxidase: immunological cross-reactivity and structural relationship to ferrochelatase. Biochim Biophys Acta 913:349–358.
180. Ferreira GC, Dailey HA (1988) Mouse protoporphyrinogen oxidase. Kinetic parameters and demonstration of inhibition by bilirubin. Biochem J 250:597–603.
181. Camadro JM, Labbe P (1996) Cloning and characterization of the yeast *HEM14* gene coding for protoporphyrinogen oxidase, the molecular target of diphenyl ether-type herbicides. J Biol Chem 271:9120–9128.
182. Dailey TA, Dailey HA (1997) Expression, purification, and characteristics of mammalian protoporphyrinogen oxidase. Methods Enzymol 281:340–349.
183. Lermontova I, Kruse E, Mock HP, Grimm B (1997) Cloning and characterization of a plastidal and a mitochondrial isoform of tobacco protoporphyrinogen IX oxidase. Proc Natl Acad Sci USA 94:8895–8900.
184. Hansson M, Gustafsson MC, Kannangara CG, Hederstedt L (1997) Isolated *Bacillus subtilis* HemY has coproporphyrinogen III to coproporphyrin III oxidase activity. Biochim Biophys Acta 1340:97–104.
185. Dailey HA, Dailey TA (1996) Protoporphyrinogen oxidase of *Myxococcus xanthus*. Expression, purification, and characterization of the cloned enzyme. J Biol Chem 271:8714–8718.
186. Wang KF, Dailey TA, Dailey HA (2001) Expression and characterization of the terminal heme synthetic enzymes from the hyperthermophile *Aquifex aeolicus*. FEMS Microbiol Lett 202:115–119.
187. Corrigall AV, Siziba KB, Maneli MH, Shephard EG, Ziman M, Dailey TA, Dailey HA, Kirsch RE, Meissner PN (1998) Purification of and kinetic studies on a cloned protoporphyrinogen oxidase from the aerobic bacterium *Bacillus subtilis*. Arch Biochem Biophys 358:251–256.
188. Heinemann IU, Diekmann N, Masoumi A, Koch M, Messerschmidt A, Jahn M, Jahn D (2007) Functional definition of the tobacco protoporphyrinogen IX oxidase substrate-binding site. Biochem J 402:575–580.
189. Jacobs NJ, Jacobs JM (1981) Protoporphyrinogen oxidation in *Rhodopseudomonas spheroides*, a step in heme and bacteriochlorophyll synthesis. Arch Biochem Biophys 211:305–311.
190. Sasarman A, Chartrand P, Lavoie M, Tardif D, Proschek R, Lapointe C (1979) Mapping of a new *hem* gene in *Escherichia coli* K12. J Gen Microbiol 113: 297–303.
191. Sasarman A, Letowski J, Czaika G, Ramirez V, Nead MA, Jacobs JM, Morais R (1993) Nucleotide sequence of the *hemG* gene involved in the protoporphyrinogen oxidase activity of *Escherichia coli* K12. Can J Microbiol 39:1155–1161.
192. Boynton TO, Daugherty LE, Dailey TA, Dailey HA (2009) Identification of *Escherichia coli* HemG as a novel, menadione-dependent flavodoxin with protoporphyrinogen oxidase activity. Biochemistry 48:6705–6711.
193. Ashenbrucker H, Cartwright GE, Goldberg A, Wintrobe MM (1956) Studies on the biosynthesis of heme *in vitro* by avian erythrocytes. Blood 11:821–833.
194. Dailey HA, Dailey TA, Wu CK, Medlock AE, Wang KF, Rose JP, Wang BC (2000) Ferrochelatase at the millennium: structures, mechanisms and [2Fe-2S] clusters. Cell Mol Life Sci 57:1909–1926.
195. Taketani S, Tokunaga R (1981) Rat liver ferrochelatase. Purification, properties, and stimulation by fatty acids. J Biol Chem 256:12748–12753.
196. Grzybowska E, Gora M, Plochocka D, Rytka J (2002) *Saccharomyces cerevisiae* ferrochelatase forms a homodimer. Arch Biochem Biophys 398:170–178.
197. Hansson M, Hederstedt L (1994) Purification and characterization of a water-soluble ferrochelatase from *Bacillus subtilis*. Eur J Biochem 220:201–208.
198. Dailey HA, Finnegan MG, Johnson MK (1994) Human ferrochelatase is an iron-sulfur protein. Biochemistry 33:403–407.
199. Day AL, Parsons BM, Dailey HA (1998) Cloning and characterization of *Gallus* and *Xenopus* ferrochelatases: presence of the [2Fe-2S] cluster in nonmammalian ferrochelatase. Arch Biochem Biophys 359:160–169.
200. Dailey TA, Dailey HA (2002) Identification of [2Fe-2S] clusters in microbial ferrochelatases. J Bacteriol 184: 2460–2464.
201. Shepherd M, Dailey TA, Dailey HA (2006) A new class of [2Fe-2S]-cluster-containing protoporphyrin (IX) ferrochelatases. Biochem J 397:47–52.
202. Cornah JE, Roper JM, Pal Singh D, Smith AG (2002) Measurement of ferrochelatase activity using a novel assay suggests that plastids are the major site of haem biosynthesis in both photosynthetic and non-photosynthetic cells of pea (*Pisum sativum L.*). Biochem J 362:423–432.
203. De Matteis F, Gibbs AH, Harvey C (1985) Studies on the inhibition of ferrochelatase by N-alkylated dicarboxylic porphyrins. Steric factors involved and evidence that the inhibition is reversible. Biochem J 226: 537–544.
204. Medlock AE, Carter M, Dailey TA, Dailey HA, Lanzilotta WN (2009) Product release rather than chelation determines metal specificity for ferrochelatase. J Mol Biol 393:308–319.
205. Hunter GA, Sampson MP, Ferreira GC (2008) Metal ion substrate inhibition of ferrochelatase. J Biol Chem 283:23685–23691.
206. Karlberg T, Hansson MD, Yengo RK, Johansson R, Thorvaldsen HO, Ferreira GC, Hansson M, Al-Karadaghi S (2008) Porphyrin binding and distortion and substrate specificity in the ferrochelatase reaction: the role of active site residues. J Mol Biol 378:1074–1083.
207. Al-Karadaghi S, Franco R, Hansson M, Shelnutt JA, Isaya G, Ferreira GC (2006) Chelatases: distort to select? Trends Biochem Sci 31:135–142.
208. Wang Y, Shen Y, Ryde U (2009) QM/MM study of the insertion of metal ion into protoporphyrin IX by ferrochelatase. J Inorg Biochem 103:1680–1686.

209. Sigfridsson E, Ryde U (2003) The importance of porphyrin distortions for the ferrochelatase reaction. J Biol Inorg Chem 8:273–282.
210. Medlock AE, Dailey TA, Ross TA, Dailey HA, Lanzilotta WN (2007) A pi-helix switch selective for porphyrin deprotonation and product release in human ferrochelatase. J Mol Biol 373:1006–1016.
211. Sellers VM, Dailey TA, Dailey HA (1998) Examination of ferrochelatase mutations that cause erythropoietic protoporphyria. Blood 91:3980–3985.
212. Luer C, Schauer S, Mobius K, Schulze J, Schubert WD, Heinz DW, Jahn D, Moser J (2005) Complex formation between glutamyl-tRNA reductase and glutamate-1-semialdehyde 2,1-aminomutase in *Escherichia coli* during the initial reactions of porphyrin biosynthesis. J Biol Chem 280:18568–18572.
213. Nogaj LA, Beale SI (2005) Physical and kinetic interactions between glutamyl-tRNA reductase and glutamate-1-semialdehyde aminotransferase of *Chlamydomonas reinhardtii*. J Biol Chem 280:24301–24307.
214. Ferreira GC, Andrew TL, Karr SW, Dailey HA (1988) Organization of the terminal two enzymes of the heme biosynthetic pathway. Orientation of protoporphyrinogen oxidase and evidence for a membrane complex. J Biol Chem 263:3835–3839.
215. Masoumi A, Heinemann IU, Rohde M, Koch M, Jahn M, Jahn D (2008) Complex formation between protoporphyrinogen IX oxidase and ferrochelatase during haem biosynthesis in *Thermosynechococcus elongatus*. Microbiology 154:3707–3714.